Geo-information Science and Remote Sensing

Thesis Report GIRS-2021-40

An Object-Based Classification Approach To Identify Pumpkin And Pumpkin Flower Using UAV Imagery

Busra Bozkurt

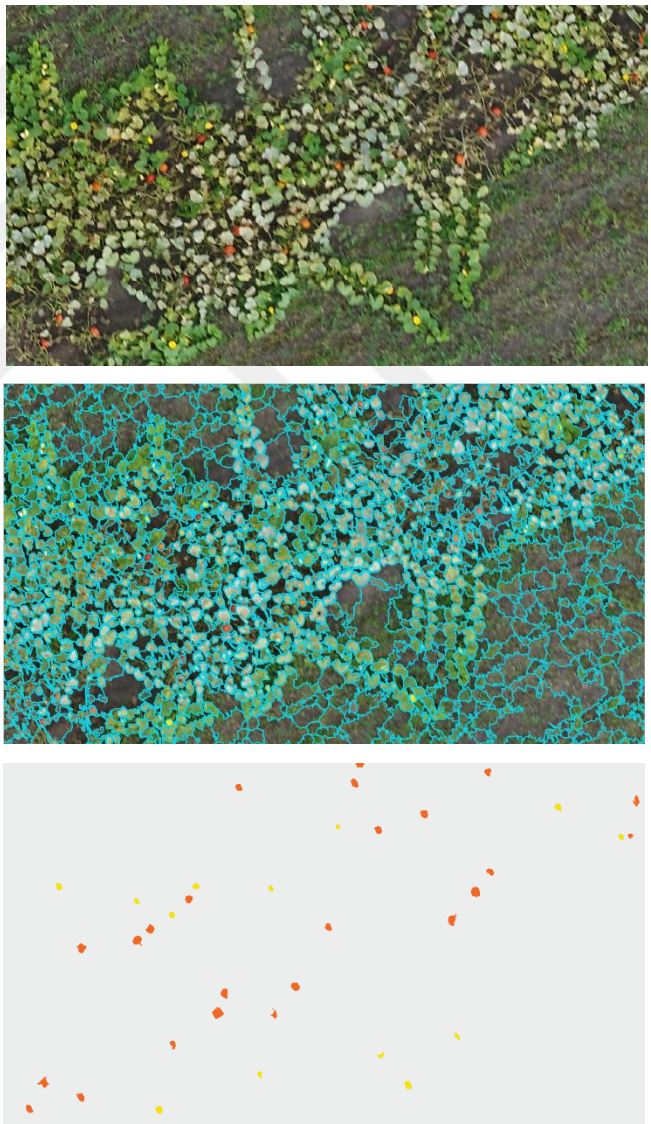

June 29th, 2021

WAGENINGEN
UNIVERSITY & RESEARCH

An Object-Based Classification Approach To Identify Pumpkin And Pumpkin Flower Using UAV Imagery

Busra Bozkurt

Student ID 1001594

Supervisor:

Dr. Ir. Lammert Kooistra

A thesis submitted in partial fulfilment of the degree of Master of Science

at Wageningen University and Research,

The Netherlands.

June 29th, 2021

Wageningen, The Netherlands

Thesis code number: GRS-80436
Thesis Report: GIRS-2021 -40
Wageningen University and Research
Laboratory of Geo-Information Science and Remote Sensing

Acknowledgments

First and foremost, I would like to thank my supervisor Lammert Kooistra for his support, guidance, and suggestions throughout this thesis journey. I really appreciate the time he has spent discussing with me in meetings and giving feedback for my report writing. I would also like to thanks Norazlida Jamil, for making the UAV data used in this study available.

In addition, a thank you to Jasper Siebring for information on image segmentation and Dainius Masiliunas who provided valuable information and help during this thesis when programming in R. The process of writing a thesis has not always been easy for me. Therefore, I want to thank all the people and supervisors of thesis ring 4 for their contribution to this thesis.

I always want to extend my gratitude to my sponsor for giving me the opportunity to study at Wageningen University. This scholarship allowed me to focus on my studies and helped me reach my goals.

Last but not least, special gratitude goes to my lovely family. To my parents and siblings, who have encouraged and supported me from a distance during my entire study. Finally, I would like to thank my friends and everybody involved in the thesis process for the support directly or indirectly.

Abstract

Crop classification via remote sensing provides important information for agricultural management. The availability of high-resolution images from unmanned aerial vehicle (UAV) offers new opportunities for crop classification. To analyze UAV imagery, crop classification based on object-based image analysis (OBIA) has been increasingly reported. Hence, the purpose of this study is to develop an OBIA approach to classify pumpkin and pumpkin flower in the heterogeneous agricultural field using UAV imagery. The approach proposed can be divided into two steps: (1) image segmentation using the Large Scale Mean-Shift (LSMS) algorithm, and (2) a classification of pumpkin and pumpkin flower by Random Forest (RF) classifier. A wide range of features, including the spectral features, textural features based on the grey-level co-occurrence matrix (GLCM), and geometric features were extracted for classification, and their contribution was evaluated with the RF variable importance measure. The results have demonstrated that the proposed object-based crop classification approach achieved a satisfactory overall accuracy of 0.94. The classification map provides a spatial distribution of pumpkin and pumpkin flower that can be used to guide farmers for agricultural management and economic purposes.

Contents

List of Figures

List of Tables

Acronyms

UAV	Unmanned Aerial Vehicle
GEOBIA	Geographic Object-Based Image Analysis
OBIA	Object-Based Image Analysis
RGB	Red-Green-Blue
LSMS	Large Scale Mean-Shift
OTB	Orfeo Toolbox
RF	Random Forest
SfM	Structure-from-Motion
DSM	Digital Surface Model
ROI	Region of Interest
GLCM	Gray Level Co-Occurrence Matrix
OOB	Out-of-Bag Observations
MDA	Mean Decrease Accuracy
MDG	Mean Decrease Gini
OA	Overall Accuracy
PA	Producer's Accuracy
UA	User's Accuracy

1. Introduction

1.1. Context and background

With the rapidly growing world population, food production needs to increase globally (FAO, 2017). This will require higher agricultural yields to meet the projected consumption demands (Foley et al., 2011). However, climate change combined with population and environmental pressures has already been hampering agricultural productivity (Waldner et al., 2015). Therefore, urgent attention must be paid to the development and sustainable management of agricultural practices to keep pace with increasing production needs (Belgiu and Csillik, 2018).

Crop mapping has become essential to effectively analyze and monitor agricultural activities and to support sustainable agricultural management (Ghazaryan et al., 2018). Accurate crop maps provide valuable information for various applications such as crop monitoring (Guan et al., 2016), yield prediction (Battude et al., 2016), and water resources management (Toureiro et al., 2017). Moreover, these crop maps are essential resources for improving decision-making processes for all stakeholders within the agricultural production chain (Liu and Bo, 2015).

Pumpkin is nowadays in peak demand with rising popularity and acreage all over the world (Kulczynski and Gramza-Michałowska, 2019; Wittstruck et al., 2021). Pumpkin farmers are exploring ways for accurate assessment of pumpkin crops to increase yield (El-Hamed and Elwan, 2011). In order to help pumpkin growers, detailed pre-harvest information about pumpkin is of great interest (Wittstruck et al., 2021). In this regard, reliable information on pumpkin derived from crop maps could offer a significant contribution to decision-makers in proper planning for management, statistical and economical purposes.

Analysis of remotely-sensed imagery provides a wide range of opportunities to address the topic of crop mapping using classification techniques (Al-Ali et al., 2020). The spatial resolution of remote sensing images is one of the most important elements for crop classification (Kwak and Park, 2019). The new generation of remote sensing platforms known as unmanned aerial vehicles (UAV) has attracted great attention in recent years due to the high spatial resolution of the sensors (Weiss et al., 2020). Compared to satellite or airborne data acquisitions, UAV are less expensive to use and a more flexible operation regarding flight planning and weather conditions (Böhler et al., 2018; Shi et al., 2016). The utilization of the UAV equipped with a digital camera is a powerful and cost-effective approach to acquire ground information in a fast and easy way (Yang et al., 2017). UAV images with very high spatial resolution improve the discrimination of various surface objects, thereby allowing to produce accurate crop maps (Kwak and Park, 2019).

Over the last decades, (geographic) object-based image analysis (GEOBIA or OBIA) has emerged as a new paradigm for analyzing very high spatial resolution imagery (Blaschke et al., 2014; Chen et al., 2018). It defines and examines objects extracted from homogeneous and contiguous pixels, which reduces intra-class spectral variability (Torres-Sánchez et al., 2015). Therefore, OBIA has proved an important approach to the use of UAV data in crop classification (Ma et al., 2017a).

1.2. Problem definition

The use of the UAV platform has made a big leap in terms of spatial resolution. With the increase in spatial resolution, single pixels no longer represent the full spatial dimension and properties of the targeted class in the image, referred to as the H-resolution case (Blaschke et al., 2014). For this reason, traditional pixel-based image classification may lead to poor results with such high spatial resolution because it analyzes individual pixels using only spectral information and does not take into account neighboring pixels (Liu and Bo, 2015). As a consequence, the classification results show a salt-and-pepper effect, and classification accuracy is reduced with traditional pixel-based image analysis with high spatial resolution images (Yu et al., 2006).

The OBIA approach is a good alternative to address the salt-and-pepper effect and H-resolution case. It first identifies homogeneous groups of neighboring pixels into meaningful image objects following a segmentation process and then uses those image objects as the basic elements for the classification (Blaschke, 2010). The OBIA method extracts not only spectral information of the pixels but also semantic properties of each object such as spatial, textural, and contextual information (Blaschke et al., 2014; Teodoro and Araujo, 2016). This makes OBIA more appropriate than pixel-based image classification in many applications, especially when using high spatial resolution data (Im et al., 2014).

Although object-based image classification has become popular in the remote sensing community over the last decades, there are potential limitations that need further exploration (Im et al., 2014). OBIA usually consists of two main phases, namely, image segmentation and feature extraction and classification. Within this framework, the object-based approach has its own limitations regarding these two aspects (Liu and Xia, 2010). Determining an optimal segmentation scale is often a challenging and crucial process commonly applied in OBIA because the resulting accuracy is directly depending on the segmentation scale (Blaschke et al., 2014). On the other hand, it is important to select the relevant features to classify the image objects in the scene for the classification result to be successful (Chen et al., 2018). Therefore, our research is performed at

multiple segmentation scales to find the optimal parameters, taking into consideration appropriate features for identifying pumpkin and pumpkin flower.

The pumpkin plant is probably the most diverse vegetable in terms of characteristics such as size, shape, and color (Kulczynski and Gramza-Michałowska, 2019). It is generally cultivated in large-scale farming areas. In that case, it is difficult to observe flowering and pumpkin crops before harvest time in large-scale heterogeneous farming areas. These issues have created challenges for pumpkin farmers to monitor pumpkin crop development and make management decisions. Hence, the identification of pumpkin and pumpkin flower is critical agronomic traits that provide beneficial information to helping farmers make optimal decisions for management and economic purposes.

Current studies have pointed out the capability of object-based analysis of UAV imagery to identify crop types, including rice (Kawamura et al., 2020), potato (Siebring et al., 2019), vegetation mapping (Oldeland et al., 2021), and almond tree flowering (López-Granados et al., 2019). Although crop classification methods based on OBIA is increasingly being reported, these methods have not been adequately tested for the detection of pumpkin and pumpkin flower using UAV data. Therefore, this thesis seeks to explore the behavior of the object-based image classification approach using high spatial resolution UAV images for pumpkin and pumpkin flower identification.

1.3. Research objectives and questions

The main objective of this thesis is to develop an object-based image analysis approach that detects pumpkin and pumpkin flower using UAV images. This approach will investigate appropriate segmentation parameters and features in order to accurately map the pumpkin and pumpkin flower. The open source software is used for image segmentation and classification to facilitate the cost-effectiveness of the research and the use of the methodology. This development will contribute to the potential of object-based analysis using UAV in the field of crop mapping.

This objective will be addressed with the following three research questions:

1. What are the suitable parameters to use for the selected segmentation algorithm?
2. Which derived features contribute to the classification of objects?
3. How accurate is the classification of the objects?

1.4. Outline

This thesis is organized into six chapters. In chapter 1, the general background and motivation of the research are introduced, followed by the research problem, research objectives, and research questions. The next chapter (2) provides a theoretical background to understand the concept of the thesis research. Chapter 3 describes the materials and methods used in this work to answer the research questions. Chapter 4 presents the results of the segmentation and classification process, while chapter 5 discusses the results by interpreting obtained results and comparing them to other similar studies. Lastly, Chapter 6 presents the conclusions, giving an overview of the results found in this thesis.

2. Related studies

2.1. Pumpkin crop

Pumpkin is an annual creeper plant belonging to the *Cucurbitaceae* plant family (Kulczynski and Gramza-Michałowska, 2019). It is a valuable vegetable crop with high productivity, high nutritive value, and good storability (El-Hamed and Elwan, 2011). The phenological period of a pumpkin crop varies between 90 to 100 days. The pumpkin growing cycle mainly consists of germination, early growth, flower development, and mature fruiting, shown in Figure 1. The growth cycle starts from seeds, and flowers develop as the plant grows and matures. Following pollination and fertilization, pumpkin fruits containing seeds develop and allow the life cycle to begin again. Hence, pumpkin seedlings consist of three main parts; green plant, flower, and fruit. Spectral reflectance of a pumpkin field may be affected by these three parts during the growing period.

Figure 1. Diagram of the pumpkin life cycle.

While growing, vegetation covers the field first, and the canopy looks green. That is why spectral reflections look similar because all plant parts are in green color. Pumpkin flowers start to bloom 8 to 10 weeks after planting. The flowers are large and bright yellow. Following pollination, pumpkin fruits begin to emerge at the bottom of the flower. Pumpkins turn color from green to orange and/or deep orange during the ripening.

Figure 2 demonstrates the spectral signatures of pumpkin, pumpkin flower, and leaves during fruit development from the image acquired from UAV equipped with a Red-Green-Blue (RGB) camera. The separability between pumpkin, pumpkin flower, and leaves is more pronounced between the Green (500-600 nm wavelength) and Red (600-700 nm wavelength) spectral regions. The pumpkin and pumpkin flower also indicate different spectral reflectance values in the Green band. However, they both show a similar spectral response, meaning that the high values in the Red band (600-700 nm wavelength) and low values in the Blue band (450-500 nm wavelength). Besides spectral reflectance, considering spatial and textural properties could provide more information to distinguish pumpkin and pumpkin flower from each other. Since pumpkin and pumpkin flower are different in size and shape, these properties could be used in order to improve pumpkin and pumpkin flower detection.

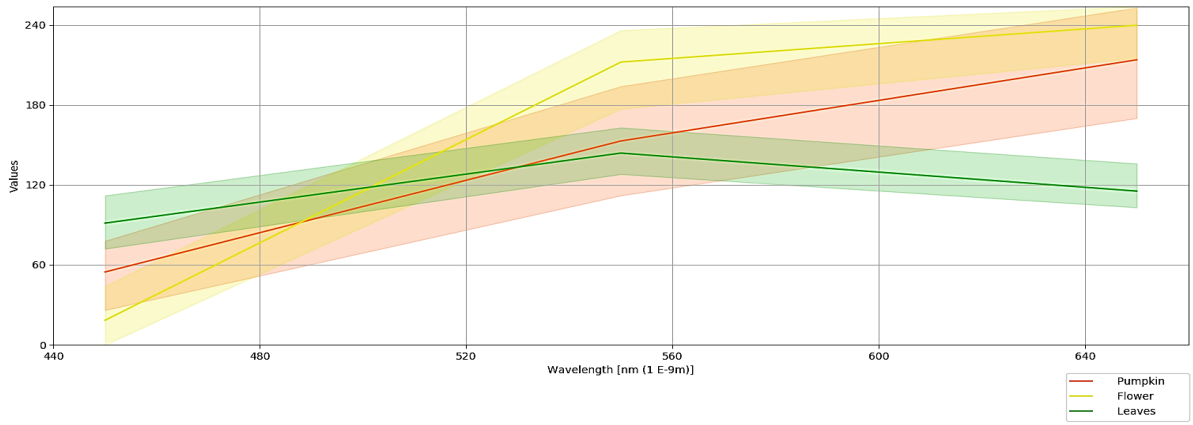

Figure 2. Spectral response of the pumpkin, pumpkin flower and leaves extracted from RGB image.

2.2. Image segmentation

Image segmentation is an initial and crucial process to produce the fundamental units of OBIA (Cheng and Han, 2016). The goal of image segmentation is to divide an image into a series of discrete regions, so-called segments or image objects that differ based on certain characteristics such as texture, color, shape, and size (Hossain and Chen, 2019). These regions represent real-world objects on the ground, corresponding to image objects in OBIA (Cheng and Han, 2016).

Segmentation algorithms commonly used for remote sensing are divided into point-based or threshold-based, edge-based, and region-based (Hossain and Chen, 2019; Kotaridis and Lazaridou, 2021; Pal and Pal, 1993). Region-based algorithms have been widely applied for segmenting remotely sensed imagery (Wang et al., 2010). Region-based algorithms try to explore the objects by growing or merging and splitting techniques based on the definition of homogeneity criteria (Blaschke et al., 2004). The advantage of the region-based methods is that segments are provided to be homogeneous spatially and/or spectrally (Wang et al., 2010).

The mean-shift algorithm is a non-parametric region merging segmentation approach that demonstrated promising results for image segmentation studies, and hence they have received the attention from remote sensing community (Huang et al., 2019; Kotaridis and Lazaridou, 2021). The Large Scale Mean-Shift (LSMS) segmentation algorithm is also a non-parametric and iterative clustering mean-shift algorithm provided by the Orfeo Toolbox (OTB) (Michel et al., 2015). It makes a group of pixels with similar meanings using the radiometric variance and mean of each band (Duarte et al., 2020; Michel et al., 2015). LSMS segmentation is notable as it allows for the optimal use of the memory and processors, and provides an open-source for remote sensing imagery processing, especially developed to be applied in large high-resolution images (De Luca et al., 2019; Duarte et al., 2020).

Little research has been carried out using LSMS segmentation using UAV images so far, but the results were promising. Duarte et al. (2020) investigated the capability of UAV imagery for detection of Eucalyptus Longhorned Borers damages in eucalyptus stands by using the LSMS segmentation algorithm. Their results showed the highest accuracy of all the models tested with 98.5% overall accuracy and 0.94 kappa value. A study by De Luca et al. (2019) focused on the reliability of the LSMS segmentation algorithm to classify cork oak woodland using UAV imagery. The supervised classifiers applied achieved a high accuracy level with overall accuracy values above 89% and kappa coefficient values of at least 0.847. There are other studies dedicating that good classification performance was achieved by LSMS segmentation, such as disease classification of potato plants (Siebring et al., 2019) and mapping the distribution of grass species (Oldeland et al., 2021).

2.3. Object-based classification

A variety of classification algorithms have been developed and implemented for remote sensing image classification. Among these algorithms available, machine learning techniques are widely utilized in order to generate reliable classification results (Ma et al., 2017b). A number of

investigations have explored the machine learning algorithms in terms of the accuracy of the classification results. The random forest (RF) classifier based on an ensemble learning technique has been proven to yield a relatively powerful technique compared to other classifiers (Belgiu and Drăgu, 2016; Song et al., 2017). Furthermore, Ma et al. (2017b) have documented a meta-analysis of the development and application of supervised object-based land-cover image classification, including various factors. They reported that RF is more efficient than other classifiers in object-based image classification.

RF offers several advantages in its application to remote sensing studies. It is a non-parametric method and therefore makes no distributional assumptions on the predictor nor response variables (Breiman, 2001). It is able to handle situations where the number of predictor variables exceeds the number of observations (Cutler et al., 2007). It is better adapted for a large volume of data and variables, and it can measure degrees of variable importance (Rodriguez-Galiano et al., 2012). These make RF algorithm a suitable classifier to perform object-based classification with a limited amount of training data and a high amount of object features.

To take advantage of the OBIA approach, object features need to be defined and calculated to use as predictor variables in the RF classification process. Besides spectral reflectance, vegetation indices, color space transformations, texture measures, and geometric features are also employed since they have been shown to be useful for object-based classification. A study by Feng et al. (2015) was presented a method combining RF and texture analysis for vegetation mapping in heterogeneous urban landscapes based on UAV data. Experimental results showed that overall accuracy for Image-A and Image-B increased from 73.5% to 90.6% and 76.6% to 86.2%, respectively, after the inclusion of texture features. The inclusion of texture features indicated that texture could greatly improve classification accuracy.

Next to texture features, color and VIs are important components humans use to recognize objects. For instance, Kawamura et al. (2020) evaluated different combinations of input features: three color spaces, canopy height model, texture, and four vegetation indices for discriminating crops/weeds in upland rice fields using UAV images with RF classifier. The results suggest that the classification accuracy was improved by combining hue-saturation-value color space with texture and spectral features. In general, the classification method of integrating spectral information with other types of features is accurate than methods that use only spectral information according to previous studies (Lee et al., 2020; Lou et al., 2020; Yu et al., 2006).

3. Materials and Methods

3.1. Overview

The proposed object-based image classification approach mainly consists of three steps, including (1) an image segmentation algorithm and quality assessment; (2) feature extraction of image objects; and (3) image classification based on the segmented objects. The methodology is summarized in Figure 3.

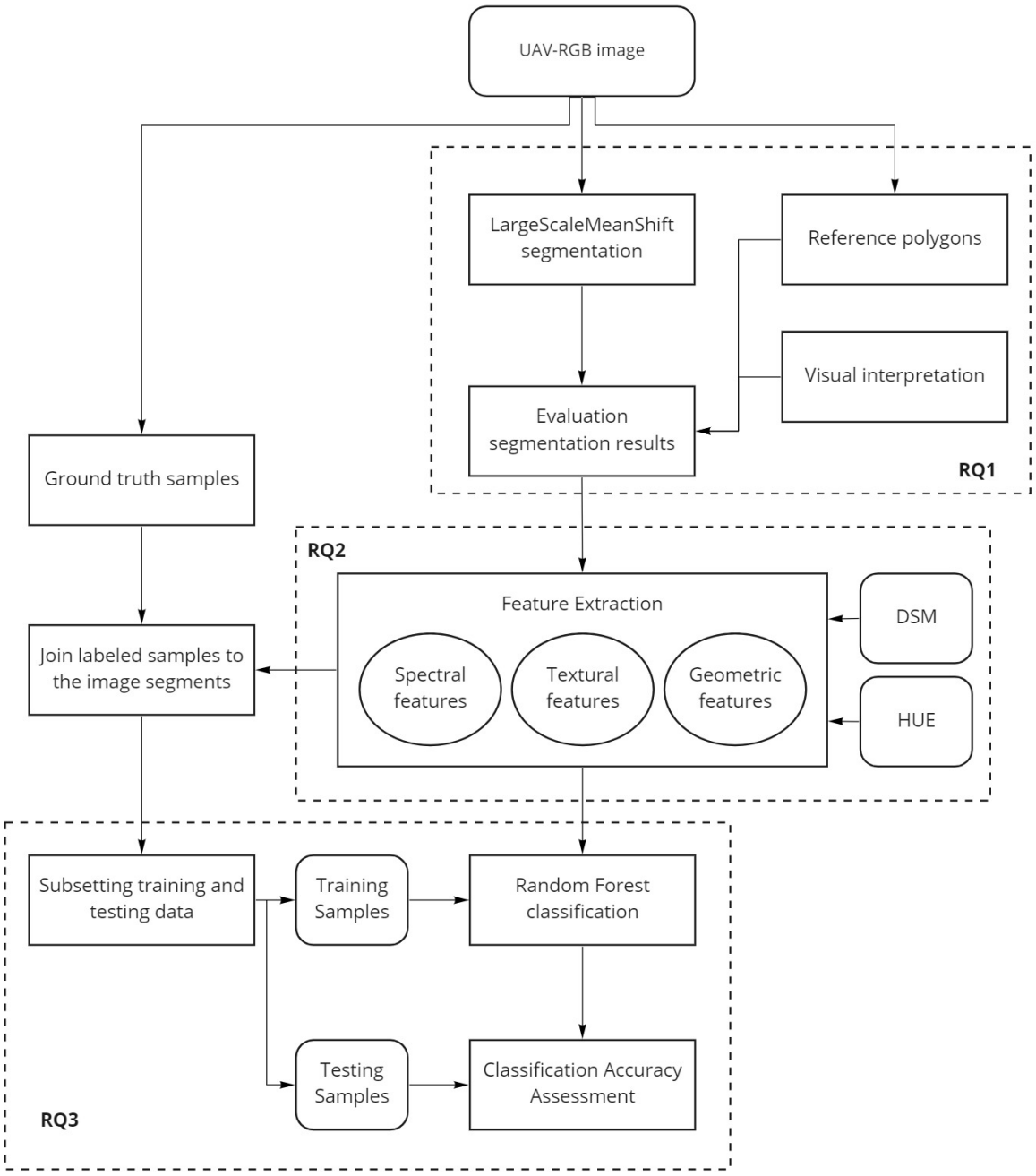

Figure 3. Schematic overview of the proposed methodology.

3.2. Study area

The study area is located within a strip cropping experiment at the Droevendaal organic experimental farm of the Wageningen University, The Netherlands (Figure 4). UAV imagery has been acquired during the 2020 growing season by Ida Norazlida, a researcher at the Farm Technology Group at Wageningen University, and dr.ir. Lammert Kooistra. There were five types of crops, including wheat, barley, potato, cabbage, and pumpkin, during the flight campaigns. This research focussed on a pumpkin field.

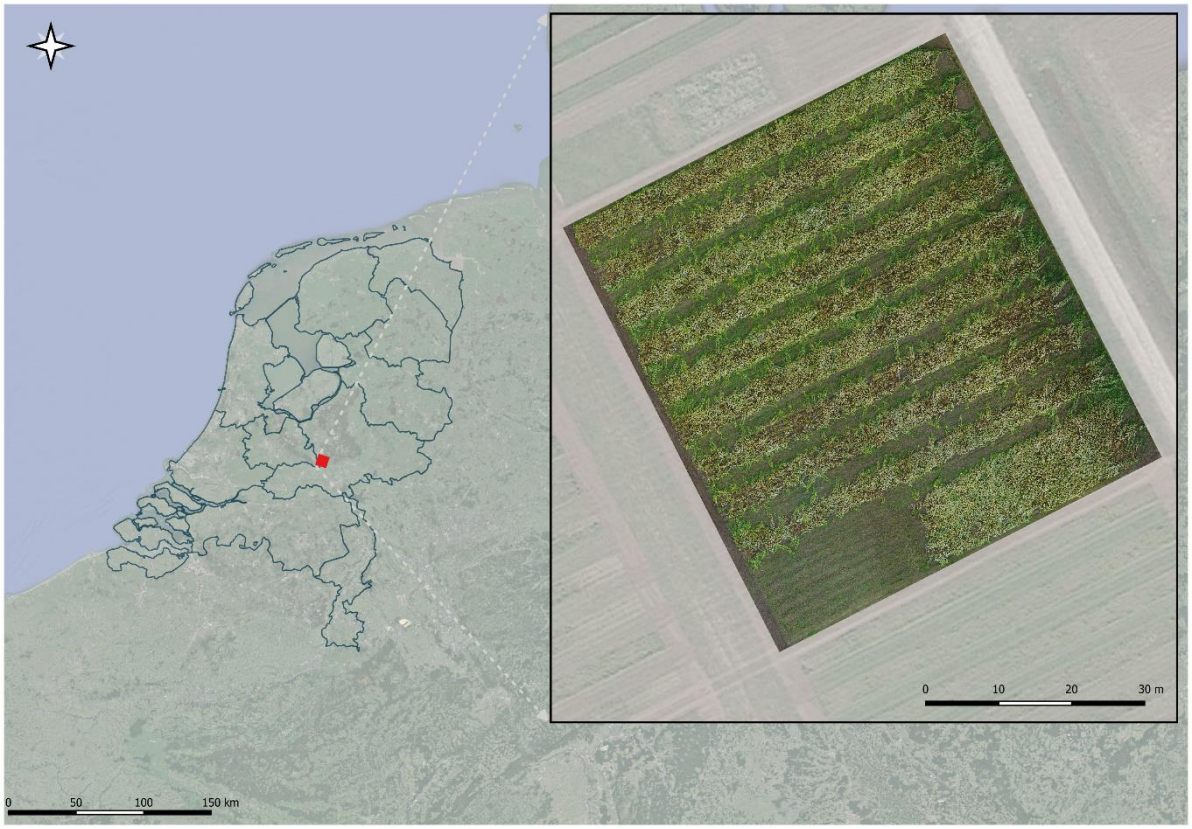

Figure 4. Map of the study area at the location of Droevendaal experimental farm in the Netherlands. The inset shows the UAV acquired RGB orthomosaic for the strip cropping field on 24-09-2020

3.3. Data description and software

3.3.1. UAV image acquisition

For the aerial survey, eleven acquisition flights were conducted within the study area, as shown in Table 1 with the growth stages of the pumpkin plant. The platform of the DJI Matrice 210, equipped with the RGB camera Zenmuse X7 was used. A flight altitude of 25 m above ground level was chosen.

Table 1.Overview of UAV campaigns and the associated development stages for the pumpkin plant.

UAV flight date	Development stages
1st July 2020	Sprout
8th July 2020	
15th July 2020	
22nd July 2020	Vine
29th July 2020	
4th August 2020	Flower development
13th August 2020	
28th August 2020	
11th September 2020	Pumpkin development
24th September 2020	
7th October 2020	

All image-based datasets have been created by Ida Norazlida. Photogrammetric and image processing procedures were carried out using Agisoft Metashape software. The raw dataset was processed using a structure-from-motion (SfM) technique, in which the identification of common features in overlapping images was performed. For geo-referencing of the UAV images, a set of 12 ground control points (GCP) were placed throughout the experimental plot. Following the geo-referencing process, RGB orthomosaic images and digital surface models (DSM) were produced. Consequently, the dataset consists of DSM and RGB orthomosaic for each flight with a spatial resolution of 6 mm. This imagery shows great potential for crop mapping at very high resolution for this heterogeneous pumpkin field.

3.3.2. Ground truth samples

The first step was to examine the orthomosaics of each flight and make a selection of images in which pumpkins and pumpkin flowers are clearly visible. Since pumpkins and pumpkin flowers are not present in the early stages of growth, the last six dates of UAV campaigns from flowering to mature pumpkin were reviewed (Figure 5). Among the available dates, the pumpkin stands out in the last two flights. However, most of the pumpkins were harvested in October. Therefore, the image of September 24 was chosen for analysis because the pumpkin is more pronounced, and pumpkin flowers are present.

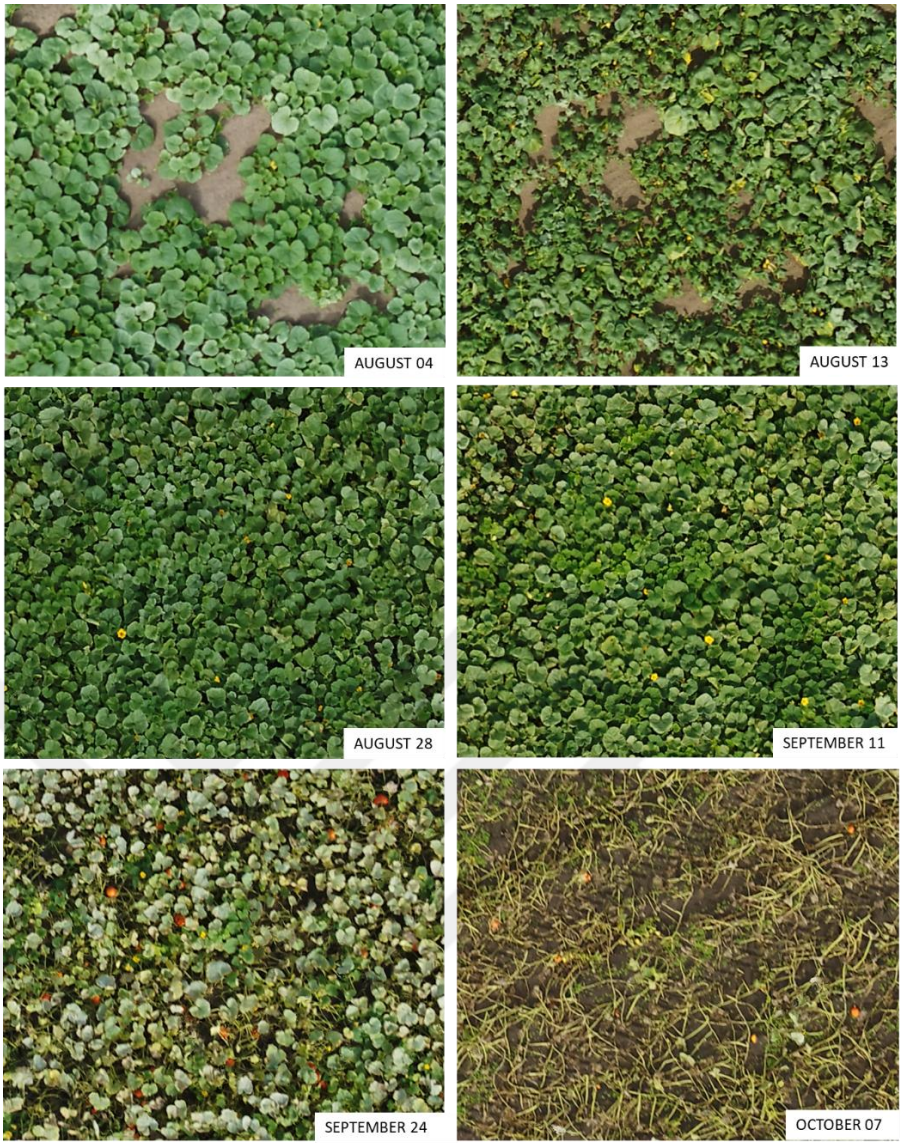

Figure 5. Illustration of RGB orthomosaics for dates from flowering to mature pumpkin development.

For the image classification, three classes were defined as pumpkin flower, pumpkin, and background that includes both leaves and soil background for the image of September 24. A total of 788 ground truth samples were manually labeled through the aid of QGIS. These samples were labeled considering location, area, shape, and color of classes. Table 2 presents a detailed description of the labeled object types for the three classes. The ground truth samples were prepared as vector points and carefully selected to ensure that all three classes are well represented.

Table 2. A detailed description of labeled object classes in the UAV-based RGB image.

Object Type	Images	Description	# of Sample Points
Pumpkin Flower		pumpkin flowers of different sizes and shapes	247
Pumpkin		pumpkins of different color, sizes, and shapes	228
Background		various and complex natural background for both leaves and soil background	370

3.3.3. Reference dataset

Initially, the total time taken to process the entire scene for image segmentation in OTB was approximately 15 hours or 20 hours. In order to reduce the processing time, two regions of interest (ROI), as illustrated in Figure 6, were defined for both pumpkin and pumpkin flower to test several segmentation parameter settings. These regions were chosen based on areas that are representing the heterogeneity of the agricultural field, such as irregularity in shape and color of pumpkin and pumpkin flower objects and their overlap with leaves or stems.

Ten reference polygons were manually digitized for pumpkin and pumpkin flower objects in the selected ROI, as seen in Figure 6. Thus, the similarity between the reference polygons and segment polygons was examined to evaluate the segmentation quality and determine the optimum segmentation parameters.

Figure 6. ROI identification with manually digitized reference polygons for pumpkin flower (a) and pumpkin (b)

3.4. Segmentation by LSMS

LSMS segmentation algorithm was adopted to generate segment regions provided by the OTB software. OTB is an open source remote sensing image processing software developed by Centre National d'Etudes Spatiales (CNES) in France (OTB Development Team, 2018). The OTB LSMS segmentation procedure consists of four steps as LSMS-smoothing, LSMS-segmentation, LSMS-merging, and LSMS-vectorization (Michel et al., 2015). It requires the setting of three parameters:

- spatial radius (spatial distance between classes)
- range radius (spectral difference between classes)
- minimum size (merging criterion)

LSMS segmentation was presented by Michel et al. (2015) as an efficient version of the mean shift segmentation, a non-parametric iterative clustering procedure by Comaniciu and Meer (2002). A detailed description of the LSMS algorithm is provided by Michel et al. (2015).

The LSMS-smoothing step is a simple iterative procedure and the first step for image segmentation. The smoothing step shifts each pixel to the average spectral signature of neighborhood pixels that are spatially closer than the spatial radius parameter and with the spectral signature with a euclidean distance to the input pixel lower than the range radius. The LSMS-segmentation step produces a labeled image where neighbor pixels whose range distance and spatial distance are below will be grouped into the same cluster. Each segmented region is then converted to a map of labeled objects.

The third step (LSMS-merging) deals with merging small objects with larger adjacent objects that has the closest radiometry. The minimum size region parameter allows the specification of the threshold for the size (in pixel) of the regions to be merged. If the segment size is lower than this threshold, the segment is merged with the segment that has the closest radiometry. The final step is LSMS-vectorization, where the segmented image is converted to a vector file with one polygon per segment.

In this work, the LSMS segmentation algorithm was applied to the two ROI separately using the UAV-RGB image of September 24. Spatial radius and range radius parameters were determined empirically by testing several segmentation settings. Starting from the default value of the spatial radius (5), the following values: 5, 10, 15, 20, and 25 were obtained. The range radius was calculated for the values between 5 and 50 with steps of 5 units.

For the minimum size region parameter, a number of small pumpkins and pumpkin flowers were measured so as to determine a suitable threshold value. This parameter was constantly kept at 100 pixels for pumpkin and pumpkin flower, as this number was the estimated minimum area of the pumpkin and pumpkin flower in pixel size. In this research, the script for the combination of different segmentation parameters was built in Python using the *otbApplication* package (OTB Development Team, 2018). This step yielded 50 segmentation results for pumpkin ROI and 50 segmentation results for pumpkin flower ROI, giving in a total of 100 segmentation results (Table 3).

Table 3. Parameter settings of the LSMS segmentation for both the pumpkin ROI and pumpkin flower ROI.

Test site	**spatial radius**	**range radius**	**minimum size**
Pumpkin ROI	5-10-15-20-25	5-50 incremented with 5	100
Pumpkin flower ROI	5-10-15-20-25	5-50 incremented with 5	100

Evaluating the performance of the segmentation algorithm plays an important role in selecting optimal scale and obtaining better segmentation results for subsequent analysis (Marpu et al., 2010). In this study, two evaluation methods were carried out to assess the quality of the segmentation results, visual interpretation and comparison based on reference polygons.

Many studies have examined the quality of image objects based on human visual inspection of image objects, and it is widely used for simplicity (Im et al., 2014). The visual interpretation was performed to describe the general segmentation result, such as delineation of targeted class and incorrect segmentation which might occur. At each setting, the segmented objects were first visually checked with the corresponding pumpkin and pumpkin flower object that could be easily interpreted in the image.

Another method is to quantitatively assess image objects with the segmentation results and the reference dataset (Wang et al., 2020). The similarity between the reference dataset and the segmented results determines the quality of the segmented image (Cai et al., 2018). A more detailed evaluation was done by comparing the segmented polygons with reference polygons through overlap analysis. Overlap analysis was implemented to calculate the percentage cover by which polygons from the segmentation layer overlap polygons from the reference layer to examine how the segmented polygons matched the manually digitized reference polygons in this study. Overlap Analysis was performed by using QGIS.

3.5. Feature extraction

After image segmentation, image objects were used to calculate features. These features per segment were utilized as input for the image classification. Due to similar spectral responses between pumpkin and pumpkin flower, it is necessary to integrate spectral, texture, and spatial information to achieve better classification results. There are totally three types of features used in this study, including 1) spectral, 2) textural, and 3) geometric. The contribution of DSM and hue has proven high classification accuracy in the previous studies (Siebring et al., 2019; Yuba et al., 2021). Hence, DSM and hue were included in this work alongside RGB for feature calculation.

Spectral features are far more frequently used for OBIA classification. Four statistical variables, brightness and yellowness index were computed for each segment (Table 4). The four statistical variables were extracted for each spectral band of RGB, DSM, and hue channel using the Zonal Statistics tool in QGIS. The brightness and yellowness index were calculated from RGB imagery.

Table 4. Description of spectral features.

Feature Type	Feature Name	Description
Spectral	Mean	The mean intensity values computed for an image segment of the RGB channels, Hue, and the DSM
	Minimum	The minimum values computed for an image segment of the RGB channels, Hue, and the DSM
	Maximum	The maximum values computed for an image segment of the RGB channels, Hue, and the DSM
	Standard Deviation	The standard deviation values computed for an image segment of the RGB channels, Hue, and the DSM
	Brightness	The average means of the RGB channels
	Yellowness Index	$\frac{Red + Green}{2} - Blue$

In high spatial resolution images, texture features are important supplementary information (Lee et al., 2020). Textures provide information on the spatial distribution of tonal variations and image structure (Haralick et al., 1973). Pumpkin and pumpkin flower show similar spectral responses but different shapes and textures. The inclusion of textural data may help improve separability between different classes with similar spectral signatures but different structures (Lee et al., 2020).

Gray level co-occurrence matrix (GLCM) is the most common statistical quantification method, and hence this study adopted the GLCM-based method for textural feature representation. The GLCM-based matrices are two-dimensional histograms of gray levels that show the probability of pixel pairs to co-occur in a given direction and at certain lag distances in an image. Eight GLCM-based statistics were computed for all directions: 0°, 45°, 90°, 135°, as defined by Haralick et al. (1973). GLCM-based variables were computed for each spectral band of RGB, DSM, and hue channel in the R software (R Core Team, 2021) using the *glcm* package (Haralick et al., 1973). The texture statistics used were as follows.

$$Mean = \sum_{i=0}^{N-1}\sum_{j=0}^{N-1} i \times P(i,j)$$

$$Variance = \sum_{i=0}^{N-1}\sum_{j=0}^{N-1} P(i,j) \times (i - Mean)^2$$

$$Homogeneity = \sum_{i=0}^{N-1}\sum_{j=0}^{N-1} \frac{P(i,j)}{1 + (i-j)^2}$$

$$Contrast = \sum_{i=0}^{N-1}\sum_{j=0}^{N-1} P(i-j)^2 P[i,j]$$

$$Angular\ Second\ Moment = \sum_{i=0}^{N-1}\sum_{j=0}^{N-1} P(i,j)^2$$

$$Correlation = \frac{\sum_{i=0}^{N-1}\sum_{j=0}^{N-1} ijP[i,j] - \mu_i\mu_j}{\vartheta_i\vartheta_j}$$

$$Entropy = \sum_{i=0}^{N-1}\sum_{j=0}^{N-1} -P(i,j) \times \ln(P(i,j))$$

$$Dissimilarity = \sum_{i=0}^{N-1}\sum_{j=0}^{N-1} P(i,j) \times |i-j|$$

where N is the number of grey levels; P is the normalized symmetric GLCM of dimension $N \times N$; $P\ (i,j)$ is the normalized grey level value in the cell i,j of the co-occurrence matrix such that the sum of $P\ (i,j)$ equals to 1 (Feng et al., 2015).

Furthermore, geometrical features are expected to improve the discriminating of the pumpkin and pumpkin flower classes since they have different properties in shape and size. There are a variety of metrics to describe the shape information of a segment; this study selected eight frequently used variables according to previous studies (Gibril et al., 2020; Lee et al., 2020) (Table 5). Polygon shape indices tool, provided by QGIS, was implemented to generate geometric features.

Table 5. Description of geometric features.

Feature Type	Feature Name	Description
Geometric	Length	The length measure of the segment.
	Width	The width measure of the segment.
	Area	It is measured by the number of pixels contained in the segment.
	Perimeter	The perimeter length of the segment.
	Maximum Distance	Maximum diameter calculated as maximum distance between two polygon part's vertices
	Shape Index	A ratio that defines border smoothness of image objects and can be computed by dividing the border length of an image object by four times the square root of its area.
	Roundness	It is expressed as the ratio of the area of the circle with a similar perimeter to the area of an image object.
	Compactness	It is expressed as the ratio of the area of an image object to the area of a circle with a similar perimeter.

3.6. Classification by Random Forest

In this study, the RF algorithm was implemented and validated using R software (R Core Team, 2021) to identify pumpkin and pumpkin flower and evaluate feature importance.

RF is an ensemble learning method that constructs multiple decision trees using random subsets taken from a training dataset through a bootstrap aggregating approach (Belgiu and Drăgu, 2016). Each classification tree is constructed from a randomly selected set consisting of approximately two-third of the training dataset. The remaining one-third portion is referred to as out-of-bag observations (OOB). The OOB of error is calculated using a one-third portion of the samples that were randomly excluded from the construction of each of the classification trees and corresponded to the rate of misclassified samples (Lebourgeois et al., 2017). OOB error is internally estimated classification accuracy that allows to validate trees and is often used to measure the generalization error on the training samples.

Another important advantage of RF is that it can measure the importance of variables by randomly permuting the value of OOB samples for a certain variable, indicating how variables will influence overall accuracy (Feng et al., 2015). RF classifier usually uses two methods to measure the importance of variables. Mean Decrease Accuracy (MDA) is the average value of decreasing accuracy of features based on OOB assessment (Pal, 2005). Mean Decrease Gini (MDG) gives the value of decreasing Gini coefficient, and it is a measure of class homogeneity (Pal, 2005). The higher the MDA value, the more important this feature is. In this research, the MDA was used to quantify how useful spectral, texture and geometric features are for pumpkin and pumpkin flower identification.

This paper has developed the RF classification model using the *caret* package (Kuhn, 2008). Tunning the RF algorithm is important in building the classification model to control the training process and hence gaining better results (Jauvin et al., 2019). In this study, two main tunning parameters in the RF model were estimated by repeated 10-fold cross-validation and grid search method. These parameters included the number of classification trees to be grown (ntree), and the number of prediction variables used in each node to make the tree grow (mtry).

The collected ground truth samples were spatially joined to image objects after the optimal image segmentation scale was identified and feature extraction (Figure 7). To establish the RF model, a set of ground truth samples was randomly divided 70% for training and 30% for testing (Table 6). First, to train the RF model, 553 image objects were randomly selected to build the classification model. The established model was then validated using 235 image objects. Section 3.5 presents all the 70 variables are used in the RF classification. Additionally, the importance of features was analyzed and compared to assess how spectral, textural, and geometric features impact classification accuracies based on the feature ranking output.

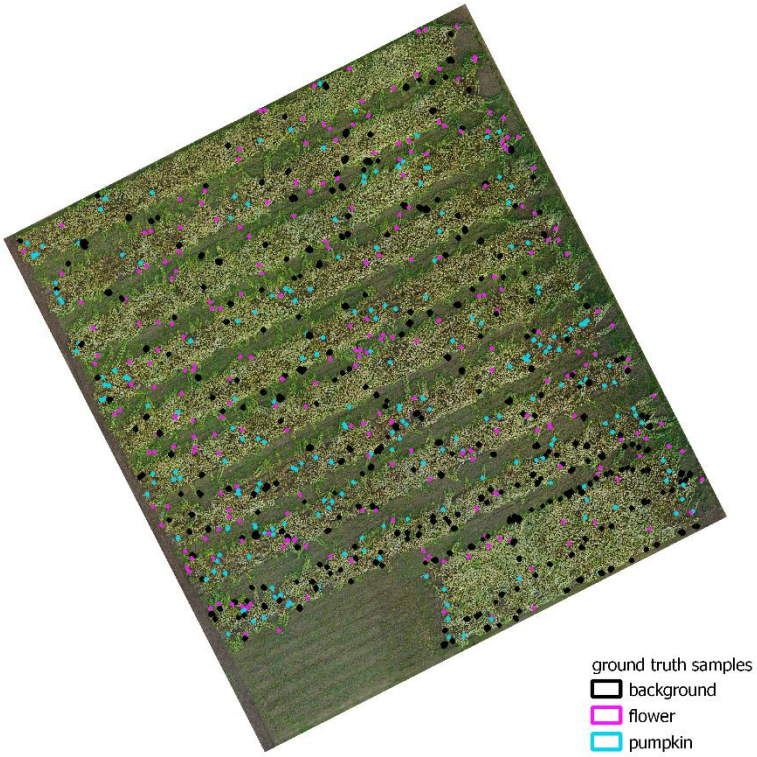

Figure 7. Spatial distribution of ground truth samples for training and testing purposes.

Table 6. Total number of training and validation objects per class.

Class	Training objects	Testing objects
background	218	93
flower	181	77
pumpkin	154	65
Total	**553**	**235**

Then the established RF model was used to predict pumpkin and pumpkin flower. Other agricultural land covers (leaves, stems, soil background) happening in the pumpkin field were also identified. The final map will provide a visual depiction of the spatial distribution of the pumpkin and pumpkin flower over the agricultural field.

3.6.1. Accuracy assessment

The validation of the RF model was carried out by doing a 10-fold cross-validation approach. This approach randomly partitions the validation objects into 10 equal subsamples. The first subsample of objects was used for testing the model and the remaining for training. Then the model was tested and trained 10 times. Each time a confusion matrix was stored in a list, then the elements in the list were calculated and combined into a final confusion matrix.

An accuracy assessment to evaluate the RF model was reported through Overall accuracy (OA), producer's accuracy (PA), and user's accuracy (UA) derived from the confusion matrix. A description of the confusion matrix and the metrics that can be derived from it can be found in Congalton (1991).

The overall accuracy is the ratio between the number of correct predictions and the total number of observations.

$$OA = \frac{\sum correct\ predictions}{total\ number\ of\ predictions}$$

where predictions were computed for all available validation objects, and the predicted classes were compared to the true classes.

The producer's accuracy value represents how well observed pixels have been classified. It is derived by dividing the number of correct pixels in one class by the number of reference pixels to be of that category.

The user's accuracy is a measure of the probability that a pixel classified into a given category actually represents on the ground. It is computed by dividing the number of correctly classified pixels in a class by the total number of pixels that were classified in that class.

4. Results

4.1. LSMS segmentation

Appropriate segmentation parameters are crucial to achieve a good segmentation result. The selection of appropriate segmentation parameters procedure is as follows: (1) define the testing ranges and the increments in every iteration for each parameter (e.g., spatial radius: 5 to 25 with an increment of 5 each time; range radius: 5 to 50 with an increment of 5), the minimum size parameter was kept constant at 100 pixels for pumpkin and pumpkin flower; (2) segment the image with each parameter combination (5 × 10 × 1 segmentations in two selected ROI); and (3) evaluate the segmentation quality of each result to select the suitable parameters. For this process, each outcome of the whole iteration procedure was assessed first using a trial-and-error approach with visual interpretation and then overlap analysis.

In general, segmentation errors can be characterized as over-segmentation and under-segmentation to specify the segmentation quality. Over-segmentation happens when a single object is segmented into smaller sub-objetcs; and under-segmentation occurs when many objects are segmented into a single segment (Marpu et al., 2010). These metrics are utilized to assess the quality of segmentation by comparing the similarity of image objects with segmented objects (El-naggar, 2018). Mismatching between segmented objects and image objects can lead to irrelevant calculated properties. In such cases, the classification model may fail to predict the class of segment objects. Therefore, image segmentation is a critical step, as segments that match the reference objects provide higher classification accuracy.

The LSMS image segmentation algorithm was tested with 50 different parameter settings in the pumpkin ROI and 50 different parameter settings in the pumpkin flower ROI. For some settings, the segmentation results seem to provide irregular segments. Low spatial and range radius values yielded many small polygons (over-segmentation), being not able to capture the pumpkin and pumpkin flower correctly. However, an increase of the spatial radius and range radius parameter led to larger polygons, which resulted in under-segmentation case. As shown in the Figure 8, segment polygons cannot adequately represent pumpkin and flower objects because of over-segmentation. In addition, flower was merged with leaves and pumpkin was also merged with stems and part of the leaves as a consequence of under-segmentation. This resulted in wrongly placed boundaries for pumpkin and pumpkin flower (Figure 8). These cases are not suitable for this study if it applies to the whole study area because very small segments and too large segments are causing confusion in the classification step.

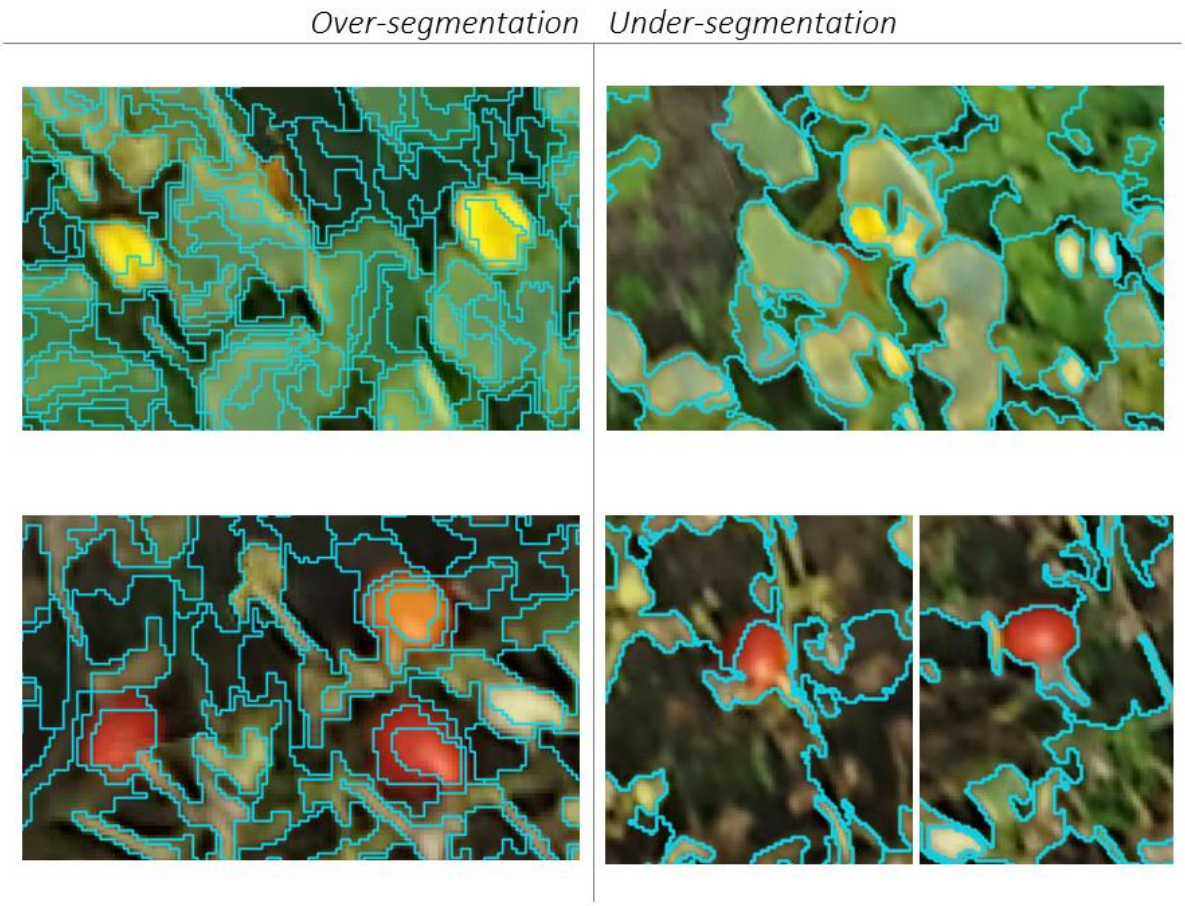

Figure 8. A section of study area showing segmentation results with spatial radius=10 and range radius=15 (left) and with spatial radius=25 and range radius=50 (right).

After visual interpretation of each setting, the segmentation evaluation through overlap analysis was carried out based on 10 reference objects for each pumpkin and pumpkin flower per ROI. The similarity was evaluated between the reference polygons and the segmented polygons derived from each setting. A good quality of segmentation result is reached when the difference between the segmentation polygons and reference polygons is low.

It can be seen that segmentation results with spatial radius=10 and range radius=15 and with spatial radius=25 and range radius=50 do not adequately cover the reference polygons (Figure 9). As a result, the difference between the segmented polygons and reference polygons is not small.

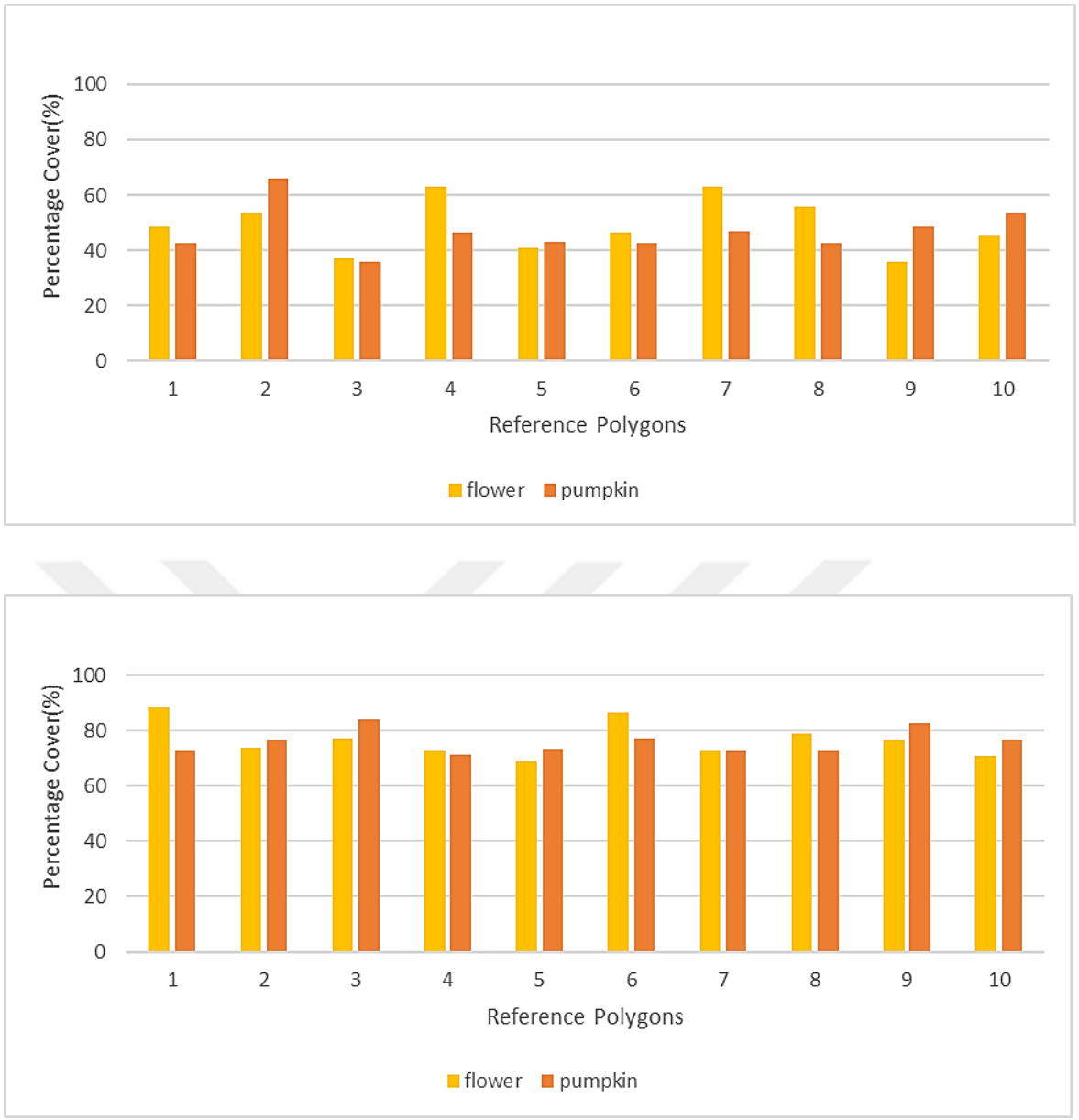

Figure 9. Overlap between reference polygons and segmented polygons generated from spatial radius=10 and range radius=15 (up) and with spatial radius=25 and range radius=50 (bottom).

The evaluation based on overlap analysis demonstrated that segmentation with spatial radius = 20 and range radius = 40 for pumpkin and pumpkin flower has successfully segmented the targeted objects with the overall difference between the references and the segmentation polygons is small (Figure 10). At this setting, the image is segmented at a finer scale, and hence these values were selected as suitable parameters for LSMS segmentation.

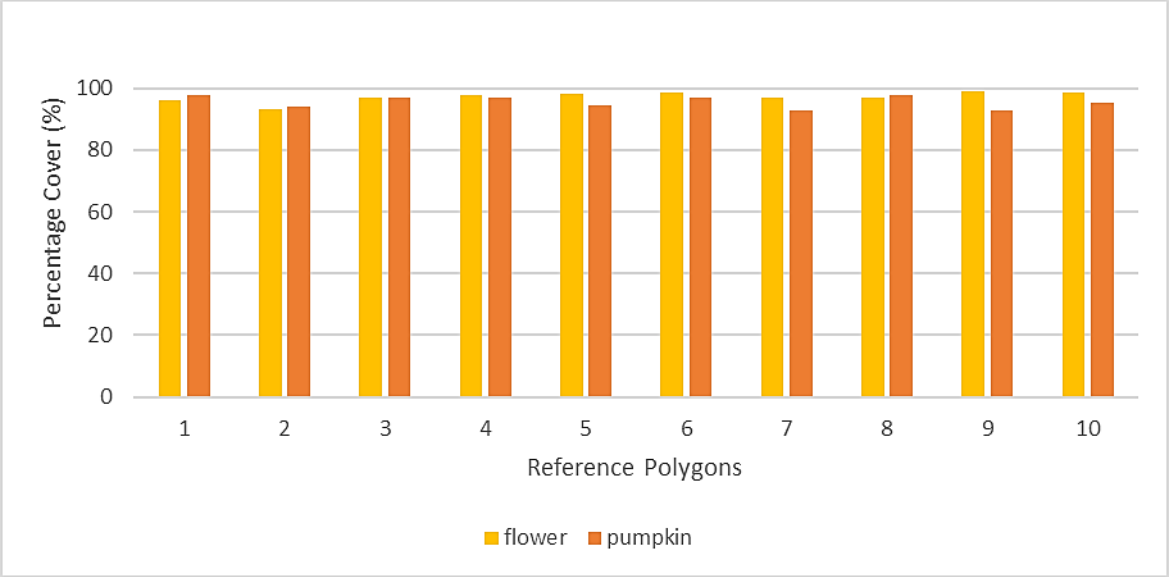

Figure 10. Overlap between reference polygons and segmented polygons generated from spatial radius of 20, range radius of 40, and minimum segment size of 100.

4.2. Random Forest classification

After the image segmentation process providing the objects to be classified, the RF model was established using training objects. The RF classifier with the optimal combinations of mtry and ntrees was identified by tuning parameters and training iterations. The best model had mtry value of 10 and ntree value of 1000 trees with the OOB estimate of error of 1.76%. This estimate of error is expressed as the number of misclassifications in the training set divided by the total number of observations.

After training the RF model, an accuracy assessment was performed to validate the classification model with the testing objects. The confusion matrix and the final model performance metrics are depicted in Figure 11 and Table 7. The result showed that the object-based classification of the UAV-RGB image achieved a satisfactory result, in which OA is 0.94. All three classes reveal a well-balanced user's and producer's accuracy. The most accurately predicted class is a flower with producer's accuracy of 0.98 and user's accuracy of 0.97, followed by background and pumpkin. Among the classes, pumpkin has the lowest producer's accuracy and user's accuracy with 0.88 and 0.90, respectively. This is because six pumpkin objects were mistakenly classified as background, and two pumpkin objects were mistakenly classified as a flower.

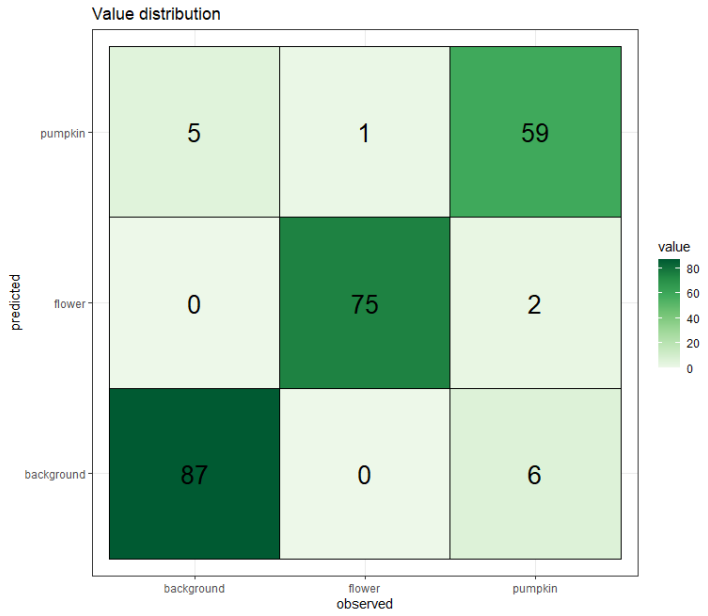

Figure 11. Confusion matrix.

Table 7. Model performance

	Producer's accuracy	**User's accuracy**
background	0.94	0.93
flower	0.98	0.97
pumpkin	0.88	0.90
Overall Accuracy = 0.94		

As a next step, the RF model was applied to the rest of the segmented objects in the whole image and assigned classes to all derived objects. Figure 12 presents the map produced through the LSMS segmentation-RF model by using the spectral, textural, and geometric features from the UAV-RGB image. This classified map allows for the identification of the pumpkin and pumpkin flower.

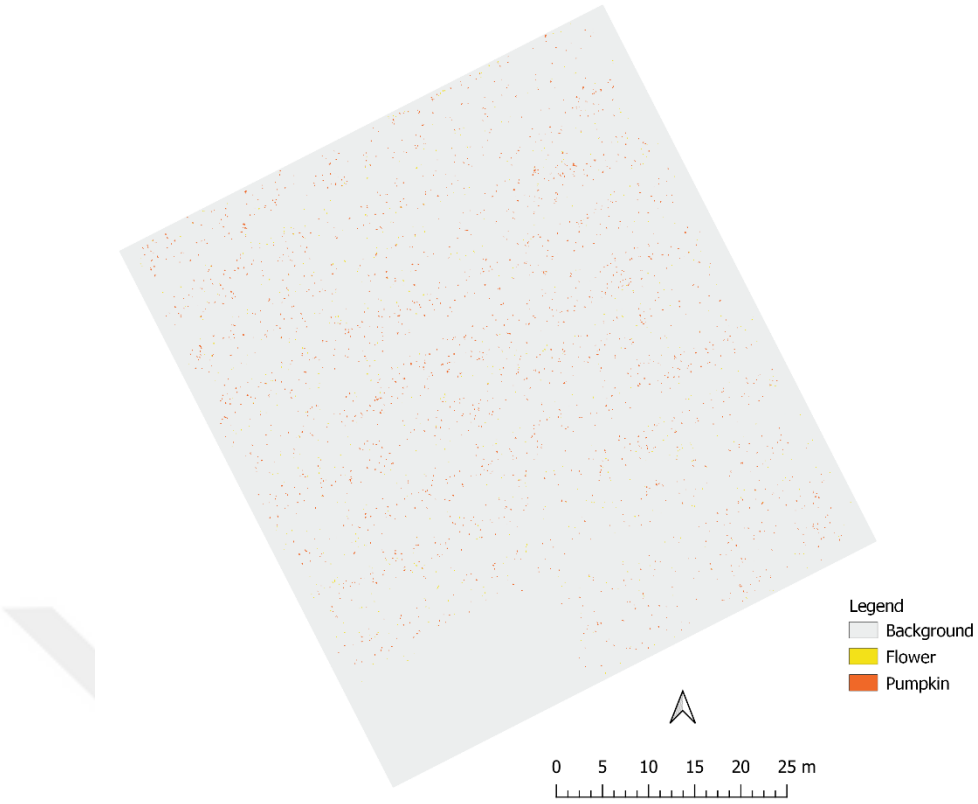

Figure 12. Classified map of RGB image using OBIA-RF classifier.

The main challenges for pumpkin and pumpkin flower detection are the heterogeneous canopy, which causes overlapping of leaves and stems and obscures the sight of pumpkin and pumpkin flower. Despite different representations of the pumpkin and pumpkin flower because of these challenges, the majority of clearly visible pumpkin and pumpkin flower were correctly classified based on the OBIA-RF classification model (Figure 13). Especially in the non-overlap areas of the pumpkin and pumpkin flower, they were classified precisely in size and shape. From visual interpretation, the disadvantage of salt-and-pepper effects from pixel-based methods is mostly eliminated in Figure 13 because OBIA treats the image in segments rather than individual pixels.

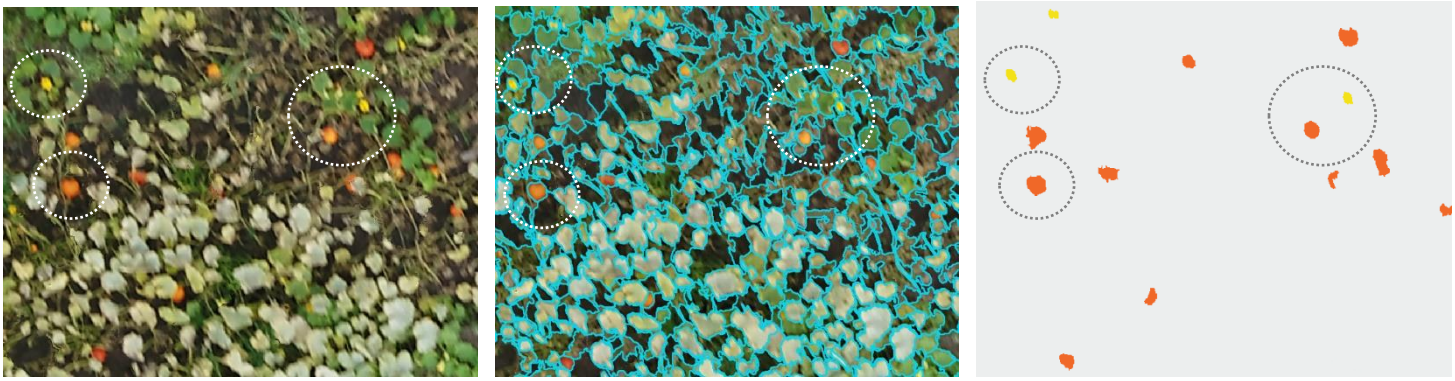

Figure 13. A subset from the study area for clear observation of non-overlap areas. (left) subset from the original image, (middle) segmentation result, (right) classification result.

However, pumpkin and pumpkin flower with overlapping areas were not adequately recognized, which were not represented pumpkin and pumpkin flower in size and shape (Figure 14). Frequently, it was also observed that nearby pumpkins were merged into single segmented objects, causing them to be classified as one object. The reason for these mismatches is that this pumpkin and pumpkin flower was partly covered by leaves.

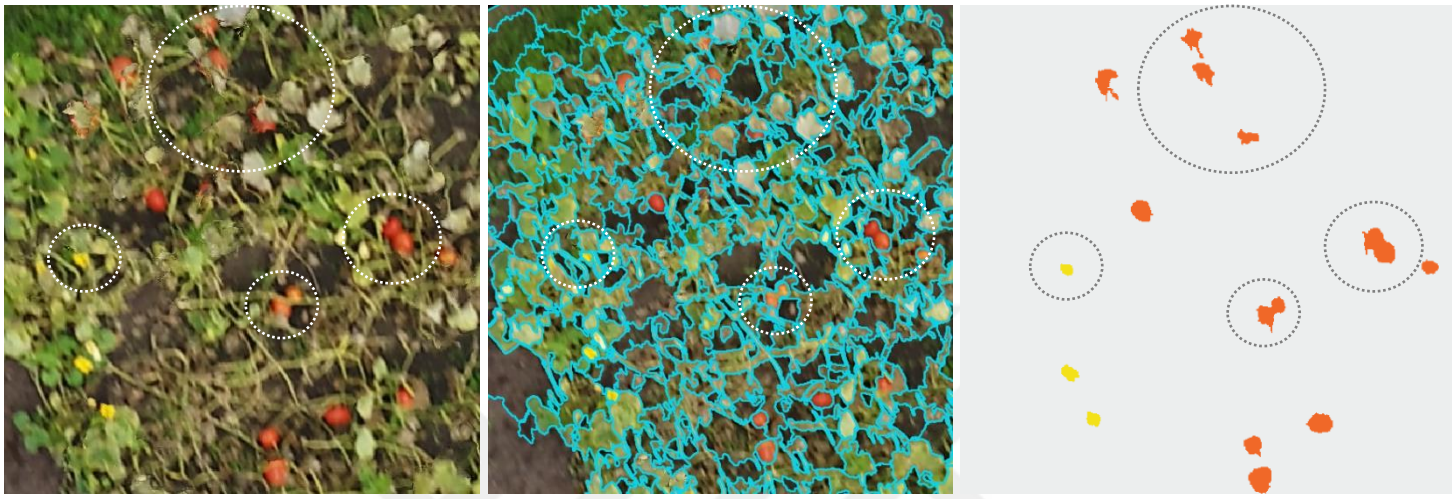

Figure 14. A subset from the study area for clear observation of pumpkin and pumpkin flower mismatches. (left) subset from the original image, (middle) segmentation result, (right) classification result.

In some cases, pumpkins were hidden under leaves, causing pumpkin objects to be mistakenly classified as background (Figure 15). It was also observed that some brightly colored small leaves were mistakenly classified as pumpkins. The main reason for these misclassifications is the high heterogeneity of the pumpkin field.

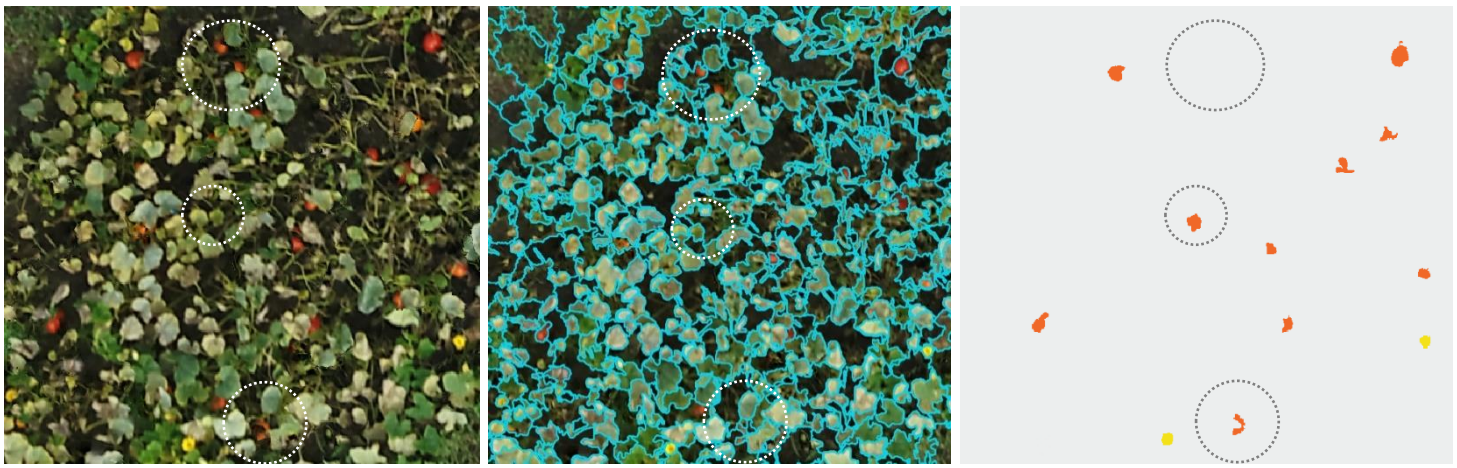

Figure 15. A subset from the study area for clear observation of overlapping areas. (left) subset from the original image, (middle) segmentation result, (right) classification result.

4.2.1. Variable importance

After extracting image objects, a total number of 70 features, including spectral, textural, and geometric features were computed. The variable importance allows determining what features are most important for pumpkin and pumpkin flower identification. See Appendix A for a detailed graph of the variable importance of all the input variables.

To further investigate the value of variables for classification, the 30 most important variables according to the MDA of input variables given by RF is depicted in Figure 16. It is obvious to note that spectral features contributed the most among the three feature types. Textural and geometric features also made useful contributions to the RF classifier.

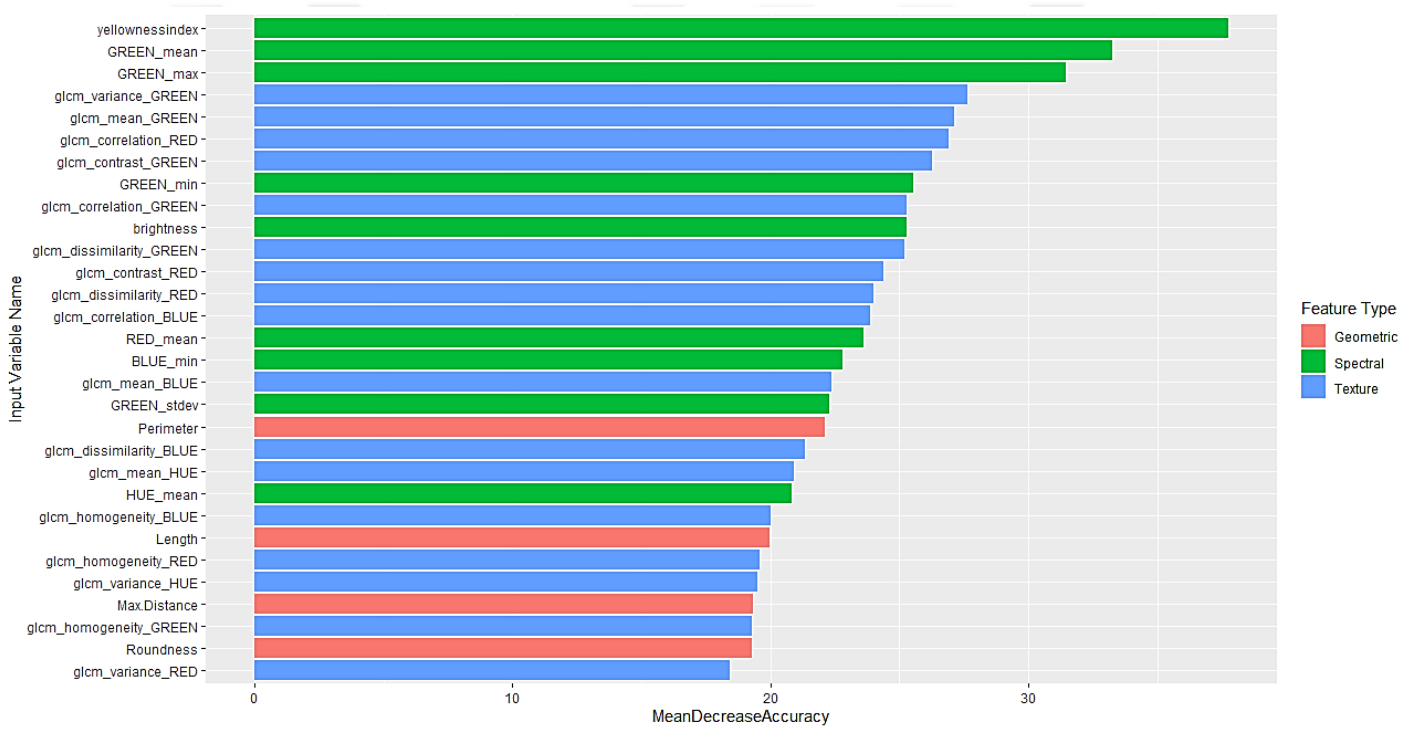

Figure 16. The top 30 variables rated by importance score in the RF classification algorithm.

Figure 16 shows that spectral reflectance values and indices were largely predominant. The best spectral feature and the most important feature is the yellowness index which is mainly because the spectral response of pumpkin and pumpkin flower is higher in the Red and Green bands than in the Blue band. From the calculated statistical variables for spectral features, mean, maximum and minimum values have the higher importance.

On the other hand, the contribution of textural features is noticeable as compared to spectral features. The dominant variables in the textural feature type are the mean and the variance values. The contribution of Red and Green channels for textural features was higher than the Blue channel. It can be noticed that some geometrical variables give high values and that the resulting additional information for pumpkin and pumpkin flower identification.

What is more, the result shows that the contribution of RGB bands to classification accuracy is generally higher than that of DSM and hue bands. In the RGB bands, the Green and Red bands have much higher importance than that of the Blue band, which is mainly because of spectral reflectance in the pumpkin field (see Section 2.1).

In summary, spectral features were the most influential in this study, and they were recommended for other related research. Aside from spectral features, textural features had distinctively high importance, which supported the usefulness of OBIA. Geometric features should be used with discretion since in this experiment, the importance of the geometric feature types was demanding attention.

5. Discussion

5.1. Image segmentation

The first research question was to identify and test the image segmentation algorithm in order to describe suitable segmentation parameters. For the identification and delineation of pumpkin and pumpkin flower in UAV imagery, the LSMS segmentation algorithm was developed based on OBIA workflow. Defining a suitable image segmentation to generate image objects is key for achieving a successful image analysis (Im et al., 2014).

The LSMS segmentation algorithm was tested in the selected ROI for pumpkin and pumpkin flower using the UAV-RGB data. The outcomes of different settings were evaluated through visual interpretation and overlap analysis. Since visual interpretation is a subjective task, reference polygons were defined to avoid errors that can arise during the segmentation process. In this study, overlap analysis was carried out to calculate the similarity between segmented polygons and reference polygons.

Over and under segmentation are a highly important issue in the segmentation process (Johnson and Xie, 2011). Similar to the work performed by Oldeland et al. (2021), the irregular behavior of the over-segmentation and under-segmentation was observed. They evaluated that an increase in the spatial radius and range radius parameters led to increasingly larger polygons, whereas low spatial radius and range radius values resulted in many small polygons.

Optimal LSMS segmentation parameters were determined the value of 20 for spatial radius, the value of 40 for range radius, and the value of 100 for minimum segment size. The segmentation outcome from this setting was highly representative for the pumpkin and pumpkin flower objects with reference polygons, as indicated in the Figure 10.

The optimal parameter setting found in this study is more or less similar in comparison to LSMS scale settings found in other studies. Most of the studies have obtained minimum size parameters by measuring a number of smaller targeted objects. De Luca et al. (2019) and Duarte et al. (2020) found parameter settings similar method by visual comparison on a different dataset. In addition, Siebring et al. (2019) calculated convex hulls for estimating spectral threshold, and they found range radius =30 and spatial radius=10.

Image segmentation is still a challenging task in OBIA. In this sense, the image segmentation process strongly depends on the image data and the purpose of the study. Since there is no standard and unique solution for the determination of the right parameter values, the segmentation continues to be a highly interactive and subjective procedure (Kotaridis and Lazaridou, 2021). Therefore, this process requires user's intervention to distinguish the different classes involved in the classification problem and must be done carefully.

A study presented by Kotaridis and Lazaridou (2021) demonstrated that almost 50% of segmentation evaluation methods rely on a qualitative visual interpretation of image objects. Similar efforts have been provided by Im et al. (2014). They reviewed a total of 76 publications in OBIA and examined the use of the segmentation scale in those publications. They found that the qualitative visual interpretation approach is a widely adopted method for the selection of optimum segmentation scale. While a simple visual interpretation approach is still commonly used to describe appropriate segmentation parameter values, a comprehensive guide should be conducted to provide the appropriate segmentation parameter value for the most used segmentation algorithms. Therefore, improvements related to optimum segmentation scale selection in OBIA within the remote sensing field should be made in the near future.

5.2. Classification results

This study explored the capability of object-based image classification in identifying pumpkin and pumpkin flower using the UAV-RGB imagery. The classification results indicate that the potential of the object-based approach in order to map pumpkin and pumpkin flower in the heterogeneous agricultural field.

In this research, the RF algorithm was used for object-based image classification. Although previous studies have implemented the RF algorithm with the default mtry number (square root of the number of input variables) and ntree (500), this thesis has optimized those parameters by tuning the RF algorithm (mtry= 10 and ntree=1000).

For complex and heterogeneous pumpkin field, the object-based image analysis method provided results with statistically significant high accuracy of overall accuracy 0.94 (Table 7). The result of this study shows higher accuracy in comparison to other studies. For example, Su and Zhang (2021) introduced an object-based RF classification framework for crop classification. Their results showed an overall accuracy of 90.52% with six classes. Furthermore, this study confirmed the

efficiency of RF classifier for crop mapping already reported in the literature (Li et al., 2015; Novelli et al., 2016).

Recently, Wittstruck et al. (2021) reported a methodology to detect and count pumpkin fruits for yield prediction using high spatial resolution UAV-RGB imagery. The issue of overlapping and adjacent pumpkin fruits were addressed by conditional and thresholding strategy to split those fruits. In this study, the attempt to identify pumpkin and pumpkin flower in the complex and heterogeneous agricultural field has been fairly successful, especially in areas where pumpkin and pumpkin flower stand with a single object and clearly visible. This study can be served as a step for more sophisticated research into crop classification in the heterogeneous and complex agricultural field.

One of the advantages of object-based classification over pixel-based classification is the ability to use additional features instead of analyzing only spectral information. Due to the availability of a large number of feature variables under the OBIA approach, selecting suitable features is important. This study highlights the most useful features for classifying pumpkin and pumpkin flower. Three types of features were extracted from each object, and a total of 70 feature variables were used in the RF classifications. Based on the importance of variables, spectral features proved to be useful for the pumpkin and pumpkin flower classification. The inclusion of texture and geometric features has provided information on the object classification that is complementary to spectral information, which is consistent with the findings of other studies (Gibril et al., 2020; Song et al., 2017).

5.3. Limitations

It is essential that the training data provide a representative description of each class to describe the image objects of the study area (Ma et al., 2015). Machine learning algorithms also require a larger number of training data for better performance (Rodriguez-Galiano et al., 2012). However, the collection of ground truth samples takes a great amount of time and effort.

The available UAV dataset is also limited for pumpkin identification. Among the available UAV images, pumpkins are more prominent only in the selected image. Therefore, a classical method from the machine learning field was chosen. The RF algorithm was chosen because it was successfully applied in the object-based image classification task.

6. Conclusions

In the past decades, methods for crop classification from UAV imagery have seen rapid advancement. Although the object-based image classification approach has been proven to provide promising results, this approach still continues to rely on user-driven knowledge because the choice of segmentation parameters requires human interpretation in some steps. Therefore, subjective assessment is a very cumbersome and time-consuming process. However, in this study, the combination of visual interpretation and overlap analysis allowed a more objective assessment of the suitability of parameter settings.

This study combined the OBIA approach and the RF machine learning method based on UAV data. The objective was to identify pumpkin and pumpkin flower in the heterogeneous and complex pumpkin field by determining the optimal segmentation scale and important features for classification. The OBIA-RF approach adopted in this study was found to be suitable for crop mapping in heterogeneous and complex farmland. The map of pumpkin and pumpkin flower could provide helpful information that can be used in decision-making systems to guide farmers for management and economic purposes.

References

Al-Ali, Z.M., Abdullah, M.M., Asadalla, N.B., Gholoum, M., 2020. A comparative study of remote sensing classification methods for monitoring and assessing desert vegetation using a UAV-based multispectral sensor. Environ. Monit. Assess. 192, 1–14. https://doi.org/10.1007/s10661-020-08330-1

Battude, M., Al Bitar, A., Morin, D., Cros, J., Huc, M., Marais Sicre, C., Le Dantec, V., Demarez, V., 2016. Estimating maize biomass and yield over large areas using high spatial and temporal resolution Sentinel-2 like remote sensing data. Remote Sens. Environ. 184, 668–681. https://doi.org/10.1016/j.rse.2016.07.030

Belgiu, M., Csillik, O., 2018. Sentinel-2 cropland mapping using pixel-based and object-based time-weighted dynamic time warping analysis. Remote Sens. Environ. 204, 509–523. https://doi.org/10.1016/j.rse.2017.10.005

Belgiu, M., Drăgu, L., 2016. Random forest in remote sensing: A review of applications and future directions. ISPRS J. Photogramm. Remote Sens. https://doi.org/10.1016/j.isprsjprs.2016.01.011

Blaschke, T., 2010. Object based image analysis for remote sensing. ISPRS J. Photogramm. Remote Sens. https://doi.org/10.1016/j.isprsjprs.2009.06.004

Blaschke, T., Burnett, C., Pekkarinen, A., 2004. Image Segmentation Methods for Object-Based Analysis and Classification, in: Remote Sensing Image Analysis: Including the Spatial Domain. Springer, pp. 211–236.

Blaschke, T., Hay, G.J., Kelly, M., Lang, S., Hofmann, P., Addink, E., Queiroz Feitosa, R., van der Meer, F., van der Werff, H., van Coillie, F., Tiede, D., 2014. Geographic Object-Based Image Analysis - Towards a new paradigm. ISPRS J. Photogramm. Remote Sens. 87, 180–191. https://doi.org/10.1016/j.isprsjprs.2013.09.014

Böhler, J.E., Schaepman, M.E., Kneubühler, M., 2018. Crop classification in a heterogeneous arable landscape using uncalibrated UAV data. Remote Sens. 10, 1282. https://doi.org/10.3390/rs10081282

Breiman, L., 2001. Random forests. Mach. Learn. 45, 5–32. https://doi.org/10.1023/A:1010933404324

Cai, L., Shi, W., Miao, Z., Hao, M., 2018. Accuracy assessment measures for object extraction from remote sensing images. Remote Sens. 10, 303. https://doi.org/10.3390/rs10020303

Chen, G., Weng, Q., Hay, G.J., He, Y., 2018. Geographic object-based image analysis (GEOBIA): emerging trends and future opportunities. GIScience Remote Sens. 55, 159–182. https://doi.org/10.1080/15481603.2018.1426092

Cheng, G., Han, J., 2016. A survey on object detection in optical remote sensing images. ISPRS J. Photogramm. Remote Sens. https://doi.org/10.1016/j.isprsjprs.2016.03.014

Comaniciu, D., Meer, P., 2002. Mean shift: A robust approach toward feature space analysis. IEEE Trans. Pattern Anal. Mach. Intell. 24, 603–619. https://doi.org/10.1109/34.1000236

Congalton, R.G., 1991. A review of assessing the accuracy of classifications of remotely sensed data. Remote Sens. Environ. 37, 35–46. https://doi.org/10.1016/0034-4257(91)90048-B

Cutler, D.R., Edwards, T.C., Beard, K.H., Cutler, A., Hess, K.T., Gibson, J., Lawler, J.J., 2007. Random forests for classification in ecology. Ecology 88, 2783–2792. https://doi.org/10.1890/07-0539.1

De Luca, G., N. Silva, J.M., Cerasoli, S., Araújo, J., Campos, J., Di Fazio, S., Modica, G., 2019. Object-Based Land Cover Classification of Cork Oak Woodlands using UAV Imagery and Orfeo ToolBox. Remote Sens. 11, 1238. https://doi.org/10.3390/rs11101238

Duarte, A., Acevedo-Muñoz, L., Gonçalves, C.I., Mota, L., Sarmento, A., Silva, M., Fabres, S., Borralho, N., Valente, C., 2020. Detection of Longhorned Borer Attack and Assessment in Eucalyptus Plantations Using UAV Imagery. Remote Sens. 12, 3153. https://doi.org/10.3390/rs12193153

El-Hamed, K.E.-S.A., Elwan, M.W.M., 2011. Dependence of Pumpkin Yield on Plant Density and Variety. Am. J. Plant Sci. 02, 636–643. https://doi.org/10.4236/ajps.2011.25075

El-naggar, A.M., 2018. Determination of optimum segmentation parameter values for extracting building from remote sensing images. Alexandria Eng. J. https://doi.org/10.1016/j.aej.2018.10.001

FAO, 2017. The Future of Food and Agriculture: Trends and Challenges.

Feng, Q., Liu, J., Gong, J., 2015. UAV Remote sensing for urban vegetation mapping using random forest and texture analysis. Remote Sens. 7, 1074–1094. https://doi.org/10.3390/rs70101074

Foley, J.A., Ramankutty, N., Brauman, K.A., Cassidy, E.S., Gerber, J.S., Johnston, M., Mueller, N.D., O'Connell, C., Ray, D.K., West, P.C., Balzer, C., Bennett, E.M., Carpenter, S.R., Hill, J., Monfreda, C., Polasky, S., Rockström, J., Sheehan, J., Siebert, S., Tilman, D., Zaks, D.P.M., 2011. Solutions for a cultivated planet. Nature 478, 337–342. https://doi.org/10.1038/nature10452

Ghazaryan, G., Dubovyk, O., Löw, F., Lavreniuk, M., Kolotii, A., Schellberg, J., Kussul, N., 2018. A rule-

based approach for crop identification using multi-temporal and multi-sensor phenological metrics. Eur. J. Remote Sens. 51, 511–524. https://doi.org/10.1080/22797254.2018.1455540

Gibril, M.B.A., Kalantar, B., Al-Ruzouq, R., Ueda, N., Saeidi, V., Shanableh, A., Mansor, S., Shafri, H.Z.M., 2020. Mapping heterogeneous urban landscapes from the fusion of digital surface model and unmanned aerial vehicle-based images using adaptive multiscale image segmentation and classification. Remote Sens. 12. https://doi.org/10.3390/rs12071081

Guan, K., Berry, J.A., Zhang, Y., Joiner, J., Guanter, L., Badgley, G., Lobell, D.B., 2016. Improving the monitoring of crop productivity using spaceborne solar-induced fluorescence. Glob. Chang. Biol. 22, 716–726. https://doi.org/10.1111/gcb.13136

Haralick, R.M., Dinstein, I., Shanmugam, K., 1973. Textural Features for Image Classification. IEEE Trans. Syst. Man Cybern. SMC-3, 610–621. https://doi.org/10.1109/TSMC.1973.4309314

Hossain, M.D., Chen, D., 2019. Segmentation for Object-Based Image Analysis (OBIA): A review of algorithms and challenges from remote sensing perspective. ISPRS J. Photogramm. Remote Sens. https://doi.org/10.1016/j.isprsjprs.2019.02.009

Huang, F., Chen, Y., Li, L., Zhou, J., Tao, J., Tan, X., Fan, G., 2019. Implementation of the parallel mean shift-based image segmentation algorithm on a GPU cluster. Int. J. Digit. Earth 12, 328–353. https://doi.org/10.1080/17538947.2018.1432709

Im, J., Quackenbush, L.J., Li, M., Fang, F., 2014. Optimum Scale in Object-Based Image Analysis, in: Scale Issues in Remote Sensing. John Wiley & Sons, Inc., Hoboken, New Jersey, pp. 197–214. https://doi.org/10.1002/9781118801628.ch10

Jauvin, M., Yan, Y., Trouvé, E., Fruneau, B., Gay, M., Girard, B., 2019. Integration of corner reflectors for the monitoring of mountain glacier areas with Sentinel-1 time series. Remote Sens. 11, 895. https://doi.org/10.3390/rs11080895

Johnson, B., Xie, Z., 2011. Unsupervised image segmentation evaluation and refinement using a multi-scale approach. ISPRS J. Photogramm. Remote Sens. 66, 473–483. https://doi.org/10.1016/j.isprsjprs.2011.02.006

Kawamura, K., Asai, H., Yasuda, T., Soisouvanh, P., Phongchanmixay, S., 2020. Discriminating crops/weeds in an upland rice field from UAV images with the SLIC-RF algorithm. Plant Prod. Sci. 1–18. https://doi.org/10.1080/1343943X.2020.1829490

Kotaridis, I., Lazaridou, M., 2021. Remote sensing image segmentation advances: A meta-analysis. ISPRS J. Photogramm. Remote Sens. 173, 309–322.

https://doi.org/10.1016/j.isprsjprs.2021.01.020

Kuhn, M., 2008. Building predictive models in R using the caret package. J. Stat. Softw. 28, 1–26. https://doi.org/10.18637/jss.v028.i05

Kulczynski, B., Gramza-Michałowska, A., 2019. The Profile of Carotenoids and Other Bioactive Molecules in Various Pumpkin Fruits (Cucurbita maxima Duchesne) Cultivars. Molecules 24, 3212. https://doi.org/10.3390/molecules24183212

Kwak, G.H., Park, N.W., 2019. Impact of texture information on crop classification with machine learning and UAV images. Appl. Sci. 9. https://doi.org/10.3390/app9040643

Lebourgeois, V., Dupuy, S., Vintrou, É., Ameline, M., Butler, S., Bégué, A., 2017. A combined random forest and OBIA classification scheme for mapping smallholder agriculture at different nomenclature levels using multisource data (simulated Sentinel-2 time series, VHRS and DEM). Remote Sens. 9, 1–20. https://doi.org/10.3390/rs9030259

Lee, R.Y., Chang, K.C., Ou, D.Y., Hsu, C.H., 2020. Evaluation of crop mapping on fragmented and complex slope farmlands through random forest and object-oriented analysis using unmanned aerial vehicles. Geocarto Int. 35, 1293–1310. https://doi.org/10.1080/10106049.2018.1559886

Li, Q., Wang, C., Zhang, B., Lu, L., 2015. Object-based crop classification with Landsat-MODIS enhanced time-series data. Remote Sens. 7, 16091–16107. https://doi.org/10.3390/rs71215820

Liu, D., Xia, F., 2010. Assessing object-based classification: Advantages and limitations. Remote Sens. Lett. 1, 187–194. https://doi.org/10.1080/01431161003743173

Liu, X., Bo, Y., 2015. Object-based crop species classification based on the combination of airborne hyperspectral images and LiDAR data. Remote Sens. 7, 922–950. https://doi.org/10.3390/rs70100922

López-Granados, F., Torres-Sánchez, J., Jiménez-Brenes, F.M., Arquero, O., Lovera, M., De Castro, A.I., 2019. An efficient RGB-UAV-based platform for field almond tree phenotyping: 3-D architecture and flowering traits. Plant Methods 15, 160. https://doi.org/10.1186/s13007-019-0547-0

Lou, P., Fu, B., He, H., Li, Y., Tang, T., Lin, X., Fan, D., Gao, E., 2020. An optimized object-based random forest algorithm for marsh vegetation mapping using high-spatial-resolution GF-1 and ZY-3 data. Remote Sens. 12. https://doi.org/10.3390/RS12081270

Ma, L., Cheng, L., Li, M., Liu, Y., Ma, X., 2015. Training set size, scale, and features in Geographic Object-Based Image Analysis of very high resolution unmanned aerial vehicle imagery. ISPRS J. Photogramm. Remote Sens. 102, 14–27. https://doi.org/10.1016/j.isprsjprs.2014.12.026

Ma, L., Fu, T., Blaschke, T., Li, M., Tiede, D., Zhou, Z., Ma, X., Chen, D., 2017a. Evaluation of feature selection methods for object-based land cover mapping of unmanned aerial vehicle imagery using random forest and support vector machine classifiers. ISPRS Int. J. Geo-Information 6. https://doi.org/10.3390/ijgi6020051

Ma, L., Li, M., Ma, X., Cheng, L., Du, P., Liu, Y., 2017b. A review of supervised object-based land-cover image classification. ISPRS J. Photogramm. Remote Sens. https://doi.org/10.1016/j.isprsjprs.2017.06.001

Marpu, P.R., Neubert, M., Herold, H., Niemeyer, & I., 2010. Enhanced evaluation of image segmentation results. J. Spat. Sci. 55, 55–68. https://doi.org/10.1080/14498596.2010.487850

Michel, J., Youssefi, D., Grizonnet, M., 2015. Stable mean-shift algorithm and its application to the segmentation of arbitrarily large remote sensing images. IEEE Trans. Geosci. Remote Sens. 53, 952–964. https://doi.org/10.1109/TGRS.2014.2330857

Novelli, A., Aguilar, M.A., Nemmaoui, A., Aguilar, F.J., Tarantino, E., 2016. Performance evaluation of object based greenhouse detection from Sentinel-2 MSI and Landsat 8 OLI data: A case study from Almería (Spain). Int. J. Appl. Earth Obs. Geoinf. 52, 403–411. https://doi.org/10.1016/j.jag.2016.07.011

Oldeland, J., Revermann, R., Luther-Mosebach, J., Buttschardt, T., Lehmann, J.R.K., 2021. New tools for old problems — comparing drone- and field-based assessments of a problematic plant species. Environ. Monit. Assess. 193, 1–14. https://doi.org/10.1007/s10661-021-08852-2

OTB Development Team, 2018. OTB CookBook Documentation.

Pal, M., 2005. Random forest classifier for remote sensing classification. Int. J. Remote Sens. 26, 217–222. https://doi.org/01431160412331269698

Pal, N.R., Pal, S.K., 1993. A Review on Image Segmentation Techniques. Pattern Recognit. 29, 1767–1775.

R Core Team, 2021. R: A language and environment for statistical computing. R Foundation for Statistical Computing, Vienna, Austria [WWW Document]. URL https://www.r-project.org/ (accessed 6.19.21).

Rodriguez-Galiano, V.F., Ghimire, B., Rogan, J., Chica-Olmo, M., Rigol-Sanchez, J.P., 2012. An assessment of the effectiveness of a random forest classifier for land-cover classification. ISPRS J. Photogramm. Remote Sens. 67, 93–104. https://doi.org/10.1016/j.isprsjprs.2011.11.002

Shi, Y., Thomasson, J.A., Murray, S.C., Pugh, N.A., Rooney, W.L., Shafian, S., Rajan, N., Rouze, G., Morgan, C.L.S., Neely, H.L., Rana, A., Bagavathiannan, M. V., Henrickson, J., Bowden, E., Valasek, J., Olsenholler, J., Bishop, M.P., Sheridan, R., Putman, E.B., Popescu, S., Burks, T., Cope, D., Ibrahim, A., McCutchen, B.F., Baltensperger, D.D., Avant, R. V., Vidrine, M., Yang, C., 2016. Unmanned Aerial Vehicles for High-Throughput Phenotyping and Agronomic Research. PLoS One 11, e0159781. https://doi.org/10.1371/journal.pone.0159781

Siebring, J., Valente, J., Domingues Franceschini, M.H., Kamp, J., Kooistra, L., 2019. Object-Based Image Analysis Applied to Low Altitude Aerial Imagery for Potato Plant Trait Retrieval and Pathogen Detection. Sensors 19, 5477. https://doi.org/10.3390/s19245477

Song, Q., Hu, Q., Zhou, Q., Hovis, C., Xiang, M., Tang, H., Wu, W., 2017. In-season crop mapping with GF-1/WFV data by combining object-based image analysis and random forest. Remote Sens. 9. https://doi.org/10.3390/rs9111184

Su, T., Zhang, S., 2021. Object-based crop classification in Hetao plain using random forest. Earth Sci. Informatics 14, 119–131. https://doi.org/10.1007/s12145-020-00531-z

Teodoro, A.C., Araujo, R., 2016. Comparison of performance of object-based image analysis techniques available in open source software (Spring and Orfeo Toolbox/Monteverdi) considering very high spatial resolution data. J. Appl. Remote Sens. 10, 016011. https://doi.org/10.1117/1.jrs.10.016011

Torres-Sánchez, J., López-Granados, F., Peña, J.M., 2015. An automatic object-based method for optimal thresholding in UAV images: Application for vegetation detection in herbaceous crops. Comput. Electron. Agric. 114, 43–52. https://doi.org/10.1016/j.compag.2015.03.019

Toureiro, C., Serralheiro, R., Shahidian, S., Sousa, A., 2017. Irrigation management with remote sensing: Evaluating irrigation requirement for maize under Mediterranean climate condition. Agric. Water Manag. 184, 211–220. https://doi.org/10.1016/j.agwat.2016.02.010

Waldner, F., Canto, G.S., Defourny, P., 2015. Automated annual cropland mapping using knowledge-based temporal features. ISPRS J. Photogramm. Remote Sens. 110, 1–13. https://doi.org/10.1016/j.isprsjprs.2015.09.013

Wang, Z., Jensen, J.R., Im, J., 2010. An automatic region-based image segmentation algorithm for

remote sensing applications. Environ. Model. Softw. 25, 1149–1165. https://doi.org/10.1016/j.envsoft.2010.03.019

Wang, Z., Wang, E., Zhu, Y., 2020. Image segmentation evaluation: a survey of methods. Artif. Intell. Rev. 53, 5637–5674. https://doi.org/10.1007/s10462-020-09830-9

Weiss, M., Jacob, F., Duveiller, G., 2020. Remote sensing for agricultural applications: A meta-review. Remote Sens. Environ. 236, 111402. https://doi.org/10.1016/j.rse.2019.111402

Wittstruck, L., Kühling, I., Trautz, D., Kohlbrecher, M., Jarmer, T., 2021. UAV-based RGB imagery for hokkaido pumpkin (Cucurbita max.) detection and yield estimation. Sensors (Switzerland) 21, 1–15. https://doi.org/10.3390/s21010118

Yang, G., Liu, J., Zhao, C., Li, Zhenhong, Huang, Y., Yu, H., Xu, B., Yang, X., Zhu, D., Zhang, X., Zhang, R., Feng, H., Zhao, X., Li, Zhenhai, Li, H., Yang, H., 2017. Unmanned aerial vehicle remote sensing for field-based crop phenotyping: Current status and perspectives. Front. Plant Sci. https://doi.org/10.3389/fpls.2017.01111

Yu, Q., Gong, P., Clinton, N., Biging, G., Kelly, M., Schirokauer, D., 2006. Object-based detailed vegetation classification with airborne high spatial resolution remote sensing imagery. Photogramm. Eng. Remote Sensing 72, 799–811. https://doi.org/10.14358/PERS.72.7.799

Yuba, N., Kawamura, K., Yasuda, T., Lim, J., Yoshitoshi, R., Watanabe, N., Kurokawa, Y., Maeda, T., 2021. Discriminating Pennisetum alopecuoides plants in a grazed pasture from unmanned aerial vehicles using object-based image analysis and random forest classifier. Grassl. Sci. 67, 73–82. https://doi.org/10.1111/grs.12288

Appendix

A. Variable importance of all input variables rated by mean decrease accuracy with the RF classification algorithm.